TWO-DIMENSIONAL STEADY BOW WAVES IN WATER OF FINITE DEPTH

Thesis by

John Kao

In Partial Fulfillment of the Requirements

for the Degree of

Doctor of Philosophy

California Institute of Technology

Pasadena, California

1998

(Submitted May 4, 1998)

Acknowledgements

I wish to express my appreciation for the aid and guidance given by my advisor, Professor Theodore Yao-tsu Wu, under his supervision this study was carried out.

I extend my thanks to the past and present members of the Engineering Science group who have helped me in various ways. I am deeply indebted to the following persons: Prof. Norden E. Hwang, Duo-min Lin, Hui Liu, Sunao Murashige, Wen-dong Qu, Zheng Shen and and Jin Zhang. Their friendship and encouragement assisted me through my graduate study at Caltech.

I am also thanks Prof. Christopher E. Brennen, Prof. Thomas Y. Hou and Prof. Fredric Raichlen for their valuable discussion on this problem.

Abstract

In this study, the two-dimensional steady bow flow in water of arbitrary finite depth has been investigated. The two-dimensional bow is assumed to consist of an inclined flat plate connected downstream to a horizontal semi-infinite draft plate. The bottom of the channel is assumed to be a horizontal plate; the fluid is assumed to be invicid , incompressible; and the flow irrotational. For the angle of incidence α (held by the bow plate) lying between $0°$ and $60°$, the local flow analysis near the stagnation point shows that the angle lying between the free surface and the inclined plate , β , must always be equal to $120°$, otherwise no solution can exist. Moreover, we further find that the local flow solution does not exist if $\alpha > 60°$, and that on the inclined plate there exists a negative pressure region adjacent to the stagnation point for $\alpha < 30°$. Singularities at the stagnation point and the upstream infinity are found to have multiple branch-point singularities of irrational orders.

A fully nonlinear theoretical model has been developed in this study for evaluating the incompressible irrotational flow satisfying the free-surface conditions and two constraint equations. To solve the bow flow problem, successive conformal mappings are first used to transform the flow domain into the interior of a unit semi-circle in which the unknowns can be represented as the coefficients of an infinite series. A total error function equivalent to satisfying the Bernoulli equation is defined and solved by minimizing the error function and applying the method of Lagrange's multiplier. Smooth solutions with monotonic free surface profiles have been found and presented here for the range of $35° < \alpha < 60°$, a draft Froude number Fr_d less then 0.5 , and a water-depth Froude number Fr_h less than 0.4 .

The dependence of the solution on these key parameters is examined. As α

decreases for fixed Fr_d and Fr_h , the free surface falls off more steeply from the stagnation point. Similarly, as Fr_d increases, the free surface falls off quickly from the stagnation point, but for decreasing Fr_h it descends rather slowly towards the upstream level. As Fr_h decreases further, difficulties cannot be surmounted in finding an exact asymptotic water level at upstream infinity, which may imply difficulties in finding solutions for water of infinite depth. Our results may be useful in designing the optimum bow shape.

Contents

List of Figures

List of Tables

Chapter 1 Introduction

Beginning with studies on ship waves, fluid dynamists and naval engineers have been seeking accurate models for designs of optimum bow shapes. The linearized theory adapted to study this problem has provided limited success in describing the asymptotic flow field at distances far away from the bow. However, it generally falls short of accurately predicting the singular behaviors of the flow in a neighborhood of the stagnation point. What is required is a fully non-linear theory that can properly treat the field equation and boundary conditions accurately.

By properly satisfying the boundary conditions at the stagnation point of a two-dimensional inclined bow plate partly submerged in water of finite depth, this work presents a complete family of solutions to the fully nonlinear problem of bow waves with the free surface rising smoothly and monotonically to the stagnation point on the bow. From these solutions, we show their dependence on the angle of incidence α held by the inclined bow plate, the draft Froude number Fr_d, and the depth Froude number Fr_h .

The problem of steady 2-D bow wave on water of infinite depth was studied by Dangan and Tulin (1972) by using a two-term expansion in powers of small Froude number. In Dangan and Tulin's problem, the bow shape was formed by a front vertical plane connected downstream to a horizontal draft plane (the angle of incidence $\alpha = 90°$ and $\beta = 90°$). Their solutions first seem to be smooth, but there exists a very small step discontinuity located on the middle of the free surface. Vanden-Broeck & Tuck (1977) and Vanden-Broeck, Schwartz &

Tuck (1978) generalized the bow shape to consist of an inclined flat plate held at incidence angle α connected downstream to a horizontal draft plane with a sharp corner. Utilizing up to a 15-term expansion in an asymptotic series of small Froude number, Vanden-Broeck & Tuck found that their solutions always had a small discontinuity in the middle of the free surface. Subsequently, they attempted to solve the problem numerically by using the integral-equation method, finding that if the whole domain of free surface was assumed to be unknown, it is impossible to obtain converged solution. However, if an inner part of the free surface near the stagnation point was assumed to be known, their conclusion was that there always exist small waves on the upstream side of the stagnation point. (The known part was taken from the smooth part of the solutions obtained earlier.) On the other hand, if the free surface at the far field was assumed to be known, they found that the free surface would become singular at the stagnation point. In our study, we examine carefully the singularities at the stagnation point and at the far upstream, and treat the whole domain of the free surface as unknown. Furthermore, we have successfully found rapidly-convergent solutions.

For the case of water of infinite depth, Tuck & Vanden-Broeck (1985) and Madurasinghe & Tuck (1986) generalized the bow configuration to include a bulb-shaped bow of arbitrary geometry shape but still the same angle of incidence $\alpha = 90^\circ$, $\beta = 90^\circ$ and obtained solution with very-small- amplitude waves existing on the upstream side of the stagnation point. However, they made the incompatible assumption that the free surface leaves horizontally at the stagnation point. On the other hand, we find that no potential flow is possible for $\alpha = 90^\circ$.

Assuming that there is a known part in the inner region of the stagnation

point, Farrow & Tuck (1995) made more calculations and concluded that all the calculations are only accurate with an error equal to 0.001 times the wave length of the small waves. Farrow & Tuck could not find a free surface that falls off monotonically. It therefore seems that their results would be applicable to the stern waves rather than bow waves (They also found that the amplitude of the small waves arising on the upstream side mostly depends on the draft Froude number but not too much on the bow shape) . Yeung (1991) generalized the problem to provide solution for unsteady start-up flow, subsequent to Vanden-Broeck's (1989) conclusion that the bow wave problem does not possess solution for steady two- dimensional wave in water of infinite depth. However, Vanden-Broeck shows that in water of finite depth, steady state solutions can be found for draft Froude number greater than 1.22 by using a series truncation method. For high Froude numbers, Rispin and Wu (1967) and Dias & Vanden-Broeck (1993) found that solutions with jet formation exist by using either matched asymptotic expansions or a series truncation method. Tuck & Vanden-Broeck (1985) suggested a model for the bow flow with a region of high vorticity on top of irrotational flow (vortex region). Furthermore, Taneda (1974), Honji (1976) and Cole et al. (1991) obtained a vortex region on top of a potential flow by experimenting at low and moderate Froude numbers.

In this thesis, we have succeeded in finding an exact solution to the nonlinear bow wave problem with a free surface rising smoothly and monotonically to the stagnation point on the bow, without a jet or vortex formation. We investigate the bow flow with a steady free surface in front of the moving object (bow plate), which is assumed to be irrotational and possessing a velocity potential, with the

viscous effects neglected.

In view of the reported difficulties involved with the case of water of infinite depth, we consider here the case of finite water depth. For simplicity, the flow domain is bounded by a free surface, a inclined flat bow plate jointed to a horizontal draft plate, and supported beneath by a flat bottom of the channel. We are interested in the regime of small to moderate Froude numbers based on the draft and on the water depth since if the inertial effects should dominate over the gravity effects in an inner region about the stagnation, the fluid on the free surface would be pushed to form a jet, a vortex region, or an unsteady upstream advancing wave. In this study, we make very careful examination of the flow singularity and the attachment condition at the stagnation point on the bow plate where the free surface meets the bow. We also investigate the asymptotic singularity behavior of the solution at the upstream infinity.

Our local flow analysis for the stagnation region shows that the inner angle β between the free surface and the inclined plate must be equal to $120°$ for the incidence angle $\alpha < 60°$. The analysis further shows that the local flow solution does not exist for $\alpha > 60°$. Tuck & Vanden-Broeck (1985) used the incidence angle $\alpha = 90°$ for vertical bow plate in their problem. They claimed that there exists a local solution that is valid at the stagnation point, but we have discovered otherwise.

In addition, we found that there exists in our local flow analysis a negative pressure region adjacent to the stagnation point on the inclined plate within the ranges $0 < \alpha < 30°$. From such negative pressure, the inclined plate can not hold the fluid unless we supply an appropriate distribution of suction force to maintain

the fluid in contact with the inclined plate. In general, as there is no suction force furnished, the local solution exists if $30° < \alpha < 60°$, but may not physically hold for $0 < \alpha < 30°$.

In addition to the necessary condition for having the stagnation inner angle $\beta = 120°$, the singularity at the stagnation point is found to have branch- point singularities of multiple irrational orders. These singularities are required to make the free surface turn with the specified local configuration as it leaves the stagnation point. In addition, the singularity at the upstream infinity has terms with branch-point of irrational orders. Those terms make the free surface rise along the flow in a manner to render the solution exact.

There are two major approaches to solving the resulting integral equations consisted of – the Bernoulli equation and two constraint equations–that we have derived for the bow flow problem. One is based on the Boundary Integral Equation formulation (as utilized by Tuck) in which all the integral equations involve variables only on the boundaries. The second approach uses series expansion method, in which the coefficients of a series expansion for the solution are determined by satisfying the free surface boundary conditions and any complementary conditions. (Vanden-Broeck used this procedure to find solutions for different related free surface problems.) For the case of bow waves on water of finite depth, we use the series expansion method, making careful provisions to admit all the flow singularities explicitly in the expression for the series expansion (to ensure satisfying the singular behaviors at the stagnation point and at the upstream infinity) .

From the numerical results obtained for the various cases explored, we found that smooth solutions generally exist in the range of $35° < \alpha < 60°$ provided the

draft Froude number is not exceedingly large. In the other range with $\alpha < 30°$, small waves are found to appear, as a rule, upstream of the stagnation point, with their amplitude gradually falling off to zero far upstream.

A related problem is the limiting form of Stokes's highest gravity wave in water with a 120° crest corner. Olfe and Rottman (1980) claimed to have obtained the limiting form, but they did not report the accuracy of their computation. Vanden-Broeck (1986) did a similar computation but only compared the maximum wave heights without providing the wave form. Recently, Vanden-Broeck (1995) used the series expansion method to evaluate the Stokes waves up to and including the limiting form; however, the free surface profiles were not given. In Vanden-Broeck (1995) , the accuracy of the numerical results is up to the fourth decimal places. In the present numerical study, the accuracy of our solutions for the bow flow is at least up to the fourth decimal places.

In chapter 2, the problem will be formulated with giving the basic assumptions and the Bernoulli equation for the bow wave problem. In chapter 3, we will present the detailed derivation of the present theoretical model (the equations of the model are transformed by conformal mapping into different coordinate systems) . The closure of the model is accomplished with two constraint equations for prescribing geometric configurations. In chapter 4, the local flow analysis for the stagnation region is presented along with the possibility of negative pressure arising within a region on the bow plate adjacent to the stagnation point. Existence of potential flow solutions is shown for the bow plate incidence angle α lying between 30° and 60° . The singular behaviors at both the stagnation point and the upstream infinity are completely determined in this study. In chapter 5, the exact form of

the complex velocity w is given, with its singular parts explicitly singled out and with its unknown part represented by a series which is analytic, regular in the entire flow field. In chapter 6, the numerical method of minimization is used to determine the coefficients of the series and solve our model equations. In chapter 7, the numerical results are presented with discussion. A few cases (for which the global solutions can be found) are demonstrated. Chapter 8 presents the summary and conclusion of our present work.

Chapter 2 A Theory for Two-dimensional Bow Waves on Water of Finite Depth

A theoretical model is developed for two-dimensional bow waves on water of arbitrary finite depth; its physical background, basic assumptions and the model equations are presented in this chapter. In general, for a two-dimensional bow of arbitrary shape moving in a rectangular channel of variable depth, this problem would be very difficult. For simplicity, we assume that the bow is an inclined flat plate which has its lower edge connect to a horizontal draft plate, semi-infinite in length to downstream infinity. The steady two-dimensional channel has its free surface rising to stagnation on the bow plate and supported beneath by a flat, horizontal plate. This ideal, simple configuration does not change the essential features of the two-dimensional bow wave problem.

2.1 The Physical Background and the Basic Assumptions

The fluid is assumed to be incompressible invicid of constant density ρ , and the flow, irrotational; and the effect of surface tension is neglected. For a ship moving at a constant speed of few meters per second on the open ocean, the Reynolds number of the flow based on a draft depth of few meters is very large. The boundary layer on the front bow plate can then be Neglected. Hence, the invicid fluid assumption is valid. Surface tension is important only when a typical length scale of the flow is

in the order of few centimeters by Hocking (1987)and Miyata et al. (1984). For a ship moving at a constant speed greater than 5 meters per second, the free surface raises a total height greater than 1.25 meters. Therefore, the effect of surface tension can be safely ignored.

Figure 2.1 indicates the position of the steady free surface $y = \eta(x)$ and the inclined bow plate. We choose the body frame fixed at the bow as the reference. The fluid flows with a uniform velocity U from the upstream infinity (at $x = -\infty$), and a different uniform velocity U_1 under the horizontal draft plate towards the downstream infinity (at $x = \infty$). The stagnation point at which the free water surface intercepts the inclined bow is taken as the origin of the x and y-coordinates in the flow plane. The free surface begins at far upstream ($x = -\infty, y = -h$) , ascending smoothly (under the gravity acceleration g) towards the stagnation point $(x = 0, y = 0)$ over a total height $h = U^2/2g$ above the free surface at upstream infinity. The bow, whose shape has a corner at the joint of the front inclined flat plate with the horizontal draft plate, is located downstream of the stagnation point. (In our model, we assume that the bow plate is always long enough above the water surface to accommodate the stagnation point.)

As shown in Figure 2.1, the inclined bow plate is held at incidence angle α with respect to the free stream and β is the inner angle subtended by the free surface and the inclined bow plate at the stagnation point. The total height of climb of the free surface to the stagnation point is h above the free surface at the upstream infinity. H is the water depth at upstream infinity $(x = -\infty)$. In addition, d is the draft depth which is the vertical distance of the horizontal draft plate blow the free surface at upstream infinity, taken positive if downward and

negative otherwise.

2.2 The Basic Equations

In the flow domain, the motion of an incompressible fluid satisfies the equation of continuity,

$$\frac{\partial u}{\partial x} + \frac{\partial v}{\partial y} = 0, \tag{2.1}$$

where u and v are the horizontal and vertical velocity components, respectively. The flow is uniform at upstream infinity ($x = -\infty$) with constant velocity $u = U$. In the steady state, the channel flow proceeds toward the bow plate, with its free surface climbing a total height h above its initial level to the stagnation point on the bow plate. After passing the bow plate, the flow enters a passage of uniform (closed) channel of depth $(H-d)$ (d being the uniform draft of the two-dimensional "semi-infinite ship") . It is assumed to reach asymptotically a uniform stream of velocity ($u = U_1$, $v = 0$) at downstream infinity ($x = \infty$). By the continuity condition of the flow, we have

$$U_1 = \frac{U\ H}{(H-d)}. \tag{2.2}$$

We note that d could be negative even if a suction pressure is required for sustaining the flow to remain in contact with the entire draft plate.

We assume that the fluid is incompressible and invicid, and the flow, steady and irrotational. Hence, a velocity potential $\phi(x, y)$ exists, such that $u = \partial\phi/\partial x$

and $v = \partial\phi/\partial y$, which satisfies, by (2.1) ,

$$\frac{\partial^2\phi}{\partial x^2} + \frac{\partial^2\phi}{\partial y^2} = 0 \ . \tag{2.3}$$

For this steady irrotational flow, the Bernoulli equation reads

$$\frac{1}{2}(u^2 + v^2) + \frac{p(x,y)}{\rho} + gy = \frac{p_0}{\rho}, \tag{2.4}$$

where p is the pressure, ρ the constant density of the fluid, g is the constant acceleration due to gravity, and p_0 is the constant ambient pressure at the free surface. The Bernoulli constant is chosen such that the free surface terminates at the stagnation point on the bow plate at $x = 0$, $y = 0$, where $u = v = 0$ and $p = p_0$. Hence, on the free surface, $y = \eta(x)$, (2.4) becomes

$$\frac{1}{2}(u^2 + v^2) + g\ \eta(x) = 0, \quad \text{on the free surface.} \tag{2.5}$$

This equation provides the dynamic boundary condition at the free surface.

This assumed flow configuration is similar to the limiting form of Stokes's highest wave with a corner at the wave crest, except that now the bow plate is not a free surface. From this boundary condition (2.5) it readily follows that the free surface falls from the stagnation point to a finite level, say $y = -h$, at upstream infinity, such that

$$U^2 = 2gh, \quad (\text{as } x \ \to \ -\infty,\ y \ \to \ -h), \tag{2.6}$$

where h is the height by which the free surface rises above the far upstream level.

In addition, the flow also satisfies the following kinematic boundary conditions:

$$v = u\frac{\partial \eta}{\partial x}, \qquad (y = \eta(x),\ x < 0, \text{ on the free surface}) \tag{2.7}$$

$$v = -u\ \tan\alpha, \quad (y = -x\ \tan\alpha, 0 < x < (h+d)\tan\alpha, \text{ on the bow plate}) \tag{2.8}$$

$$v = 0, \quad (y = -(h+d),\ x > (h+d)\ \tan\alpha, \text{ on the draft plate}) \tag{2.9}$$

$$\text{and } v = 0\ , \qquad (\ y\ =\ -(H+h), \text{ on the channel bottom}). \tag{2.10}$$

The set of equations (2.3)-(2.10) constitutes a complicated nonlinear problem. The goal of our study is to solve the above system of equations by employing functional analysis and conformal mapping techniques togather with auxiliary computational methods.

2.3 Nondimensionalization

To simplify the evaluation, we scale all the lengths by the total free surface rise h , all the velocities by the free stream velocity U , the velocity potential ϕ by Uh , and the pressure p by ρgh (or by $\frac{1}{2}\rho U^2$) , so that we have the dimensionless variables (denoted by $\hat{}$) :

$$\hat{x} = \frac{x}{h},\ \hat{y} = \frac{y}{h},\ \hat{d} = \frac{d}{h},\ \hat{H} = \frac{H}{h},\ \hat{\eta} = \frac{\eta}{h},\ \hat{u} = \frac{u}{U},\ \hat{v} = \frac{v}{U}, \tag{2.11}$$

and,

$$\hat{\phi} = \frac{\phi}{h\ U},\ \hat{p} = \frac{p}{\rho g h} \quad . \tag{2.12}$$

In terms of these new variables, equations (2.1), (2.3), and the boundary conditions (2.7)-(2.10) retain the same form as before whilst the Bernoulli equations (2.4) and

(2.5) become

$$(\hat{u}^2 + \hat{v}^2) + \hat{p}(x, y) + \hat{y} = 0, \qquad \text{in the flow domain,} \tag{2.13}$$

$$(\hat{u}^2 + \hat{v}^2) + \hat{\eta} = 0, \quad \hat{x} < 0, \quad \text{on the free surface} \tag{2.14}$$

where the ambient pressure is set by $p_0 = 0$ as the gauge. The range of $\hat{\eta}$ is between -1 and 0 while $\hat{u}$ varies between 0 and 1 on the free surface.

Accordingly, the solution of this problem will depend on three non-dimensional parameters: the water depth $\hat{H}$, the draft $\hat{d}$, and the angle of incidence α of the bow plate. Moreover, the location of the bow-draft corner can be determined in terms of α and $\hat{d}$.

The Froude number is a ratio of the inertial effect to the gravity effect. For small Froude numbers, the gravity effect pre-dominates over the inertial effect in the flow field, except possibly in local regions where the local velocity is very large. When the Froude number is large, the inertial effect dominates over the gravity effect at least in an inner region near the bow. There are two Froude numbers which can serve useful purposes for our problem: a Froude number based on the free stream velocity U and the water depth H , F_h , and another Froude number, F_d , based on U and $(h+d)$, the vertical depth of the submerged part of the inclined bow plate from the stagnation point down to the bow-draft corner, namely

$$F_h = \frac{U}{(g\ H)^{\frac{1}{2}}}, \quad F_d = \frac{U}{(g\ (h+d))^{\frac{1}{2}}}. \tag{2.15}$$

By substituting the non-dimensional parameters (2.11)-(2.13) in (2.15) and

using (2.6) , $2gh = U^2$, we have

$$F_h = (\frac{2}{\hat{H}})^{\frac{1}{2}}, \quad F_d = (\frac{2}{1+\hat{d}})^{\frac{1}{2}} \quad . \tag{2.16}$$

Thus, the two Froude numbers are inversely proportional to the square root of $\hat{H}$ and $1 + \hat{d}$. We note that $F_d < \sqrt{2}$ provided that the draft $\hat{d} > 0$. That the Froude number F_d has this upper bound is because the bow plate is rendered long enough to admit the stagnation point to fall on the bow plate, however larger U may be. Only when the bow plate is too short to intercept the stagnation can we have a spray sheet formation at the leading edge of the bow plate, as is known for the case of high-Froude-number problem of planing plate first considered by Wagner(1932).

In this study, we shall assume that $F_d < \sqrt{2}$, though we may attempt to find solutions in the regime slightly above $F_d = \sqrt{2}$ (with the draft $d < 0$) by numerical experimentation. Furthermore, we shall assume F_h to be sufficiently smaller than unity, say $F_h < 0.3$. The critical case of $F_h = 1$ can be very singular. Under external forcing, such as by the inclined bow plate moving steadily with a transcritical velocity lying in a range $0.8 < F_h < 1.2$, say, resonant generation of upstream radiating solitary waves, periodically and incesantly, is known to occur, as was first discovered by Wu and Wu (1982) .

Within an appropriate range of the Froude numbers F_d and F_h as stated above, the solution presently sought is expected to exist in a smooth and steady state as assumed.

In the subsequent chapters, all the variables are dimensionless, and the symbol $\hat{}$ will be omitted as understood unless designated otherwise.

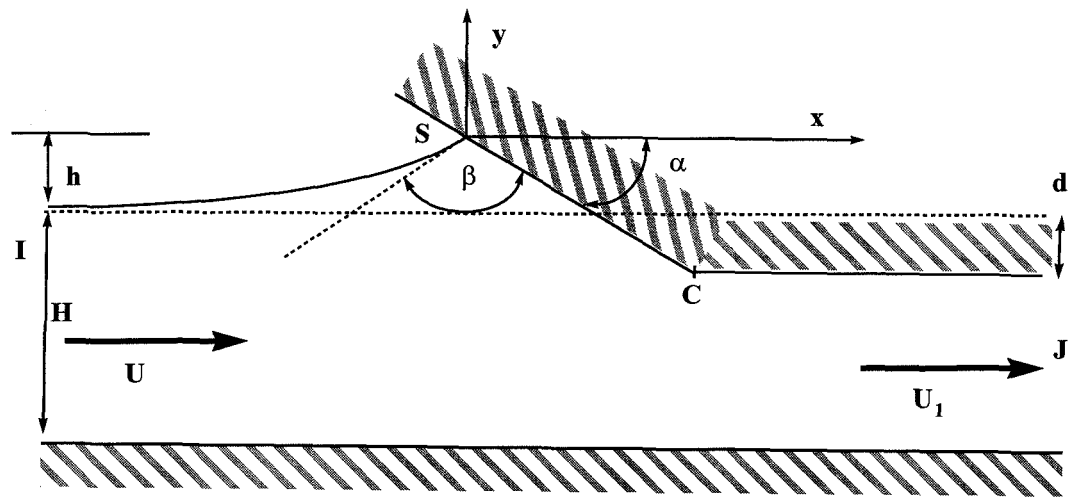

Figure 2.1: A sketch of bow flow.

Chapter 3 The Analysis and the Integral Equations

We shall solve the set of equations (2.1)-(2.10) together with (2.13, 2.14) by applying methods of complex function analysis and conformal mapping to obtain a set of nonlinear integral equations for numerical computation of the solution. By applying the method of conformal mapping, the dependent and independent variables are first interchanged with the complex potential $f = \phi + i\psi$ serving the independent variable, where ψ is the stream function conjugate to the velocity potential ϕ . The complex velocity w , where $w = u - iv = df/dz$, and the physical plane $z = x + iy = \int w^{-1}(f)\, df$, are analytic functions of f in the whole flow domain. Thus, the problem is reduced to finding a solution for $w(f)$ and $z(f)$ which also satisfies all the boundary conditions imposed on the flow.

By using a set of successive conformal transformations in complex domain, the flow is mapped into the interior of a unit semi-circle in the ζ-plane with its diameter corresponding to the solid boundaries and the semi-circle to the free surface. Within the semi-circle, the complex velocity w is analyzed as a multiplying product of two parts, $w = w_0(\zeta)\, w_c(\zeta)$, where $w_0(\zeta)$ is expressed in terms of the known branch-point singularities at the stagnation corner and at the bow-draft corner and $w_c(\zeta)$ is a complementary part which can be represented in terms of a complex series. It turns out that the complementary part w_c only has to satisfy the Bernoulli equation at the free surface and an additional constraint equation which is related to specifying the water depth H . Accordingly, application of the

Bernoulli equation gives a nonlinear integral equation, whereas invoking one of constraint conditions yields another integral equation. This set of coupled integral equations is found convenient for numerical computation of the solution.

3.1 The Conformal Transformations

We start with employing the complex variable $z = x+iy$ for the physical plane, the complex potential $f(z) = \phi + i\psi$ for the potential plane, and the complex velocity $w(z)$ for the hodograph plane, where

$$w(z) = \frac{\partial f(z)}{\partial z} = u(z) - iv(z). \tag{3.1}$$

Since the position of the free surface is unknown in the physical z-plane but is known in advance in the complex potential f-plane, we adopt the variable $f = \phi + i\psi$ instead of $z = x + iy$ as the independent variable, so that $z(f)$ is now an analytic function of f .

The flow field in the f-plane is given in Figure 3.1 . The free surface and the bow-draft plate are mapped into an infinite horizontal line, $\psi = 0$ and $-\infty < \phi < \infty$, with the stagnation point located at the origin while the channel bottom plate is mapped into the line $\psi = -Q$, where Q is the total flux $Q = UH = H$. In the f-plane, the fluid flows along $\psi =$ constant lines with a uniform velocity U from the upstream infinity (point I), and with a different uniform velocity U_1 given by (2.2) towards the downstream infinity (point J).

The complex velocity potential w can now be written as

$$\frac{1}{w(f)} = \frac{\partial z(f)}{\partial f}, \tag{3.2}$$

so that $z(f)$ is given by quadrature,

$$z = \int_0^f \frac{1}{w(f)} df, \tag{3.3}$$

with the origin $z = 0$ fixed at the stagnation point $f = 0$.

To facilitate function analysis, we next introduce a conformal transformation from the f-plane to the complex t-plane, given by

$$f = \frac{Q}{\pi} \log(\frac{t+1}{2}), \tag{3.4}$$

by which the flow domain is mapped into the lower half t-plane. The bottom plate of the channel, the free surface, and the bow-draft plate are mapped into different intervals of the real t-axis, as shown in Figure 3.2 . More specifically, the stagnation point is mapped onto $t = 1$ of the real t-axis and the upstream infinity (point I) into $t = -1$, with the free surface covering the segment between $t = -1$ and $t = 1$ of the real t-axis. The bow-draft plate is mapped into the part $t > 1$ of the real t-axis, with the bent corner mapped onto a certain point C at $t = t_C > 1$. The bottom of the channel is mapped into the part $t < -1$ of the real t-axis. The downstream infinity (point J) is mapped onto $t = \infty$. The flow enters the domain from the point $t = -1$ and goes out towards $t = \infty$ in all directions.

Next, we transform the flow domain into the upper half of the unit circle in

the ζ-plane by the conformal mapping

$$t = \frac{1}{2}(\zeta + \frac{1}{\zeta}), \tag{3.5}$$

with the flow boundary shown in Figure 3.3 . The stagnation point is mapped onto $\zeta = 1$. The point $t = \infty$ is mapped onto the origin of the ζ-plane, the point $t = -1$ onto $\zeta = -1$, and the free surface is mapped into the upper half of the unit circle $|\zeta| = 1$. The bow-draft plate is mapped into the interval $0 < \zeta < 1$ on the positive real ζ-axis, while the flat bottom of the channel is mapped into $-1 < \zeta < 0$ on the negative real ζ-axis. The flow comes in at the point $\zeta = -1$ on the real ζ-axis and exits at the origin.

For further analysis, we express the complex variable ζ in polar form, $\zeta = |\zeta| \exp(i\chi)$, where $\chi = \arg \zeta$. On the free surface, $|\zeta| = 1$, hence $\zeta = \exp(i\chi)$ with χ varying between $0°$ and $180°$, and with the corresponding t given by

$$t = \cos(\chi), \quad \text{on the free surface.} \tag{3.6}$$

The physical z-plane therefore follows accordingly as

$$z = x + iy = \frac{H}{\pi} \int_1^t \frac{1}{w(t)(t+1)} dt, \tag{3.7}$$

$$\text{or} \quad z = x + iy = \frac{H}{\pi} \int_1^\zeta \frac{(\zeta - 1)}{w(\zeta)(\zeta + 1)\zeta} d\zeta, \tag{3.8}$$

where H is the free stream water depth. In particular, position z on the free surface, by 3.6) and (3.7), is given by

$$z = x + iy = -\frac{H}{\pi} \int_0^\chi \frac{\sin(\chi)}{w(\chi)(1 + \cos(\chi))} d\chi, \quad (0 \le \chi \le \pi) \tag{3.9}$$

in which the velocity $w(\chi)$ is complex. The net result of these coordinate transformations is to map the flow domain into the upper half of the unit disk $|\zeta| \leq 1$ so that the undetermined part of $w(\zeta)$ can be expressed as a series in ζ with unknown coefficients. A similar method of coordinate transformations is used in the calculation of Stoke's highest waves with a 120° corner by Schwartz (1974) . However, the present bow-wave problem is considerably more difficult due to the presence of both free and solid flow boundaries.

3.2 Bernoulli's Equation and Constraint Conditions

We proceed to express Bernoulli's equation (2.4, 2.5) in terms of ζ . First, we have

$$u^2 + v^2 = (u - iv)(u + iv) = w\overline{w}, \tag{3.10}$$

where $\overline{w}$ is the complex conjugate of $w = u - iv$. Alternatively, in polar form, $w(\zeta) = q \ \exp(-i\theta)$, where $q = |w|$ and $\theta = -\arg w$, or

$$v/u = \tan\theta, \tag{3.11}$$

which holds throughout the flow domain and signifies, in particular, that the kinematic condition on the free surface is automatically satisfied. Alternatively henceforth, we shall also make use of the logarithmic hodograph variable,

$$\omega = \log(1/w) = \tau + i\theta \ , \quad w(\zeta) = q \ \exp(-i\theta), \quad \tau = \log(1/q). \tag{3.12}$$

In terms of θ , the kinematic boundary condition on the bow-draft plate, (2.8) and (2.9) clearly become

$$\begin{aligned} \theta &= -\alpha\,, \quad (\, c<\zeta<1,\ Im\zeta=0\,,\ \text{on the bow plate}\,) \\ \theta &= 0\,, \quad (\, 0<\zeta<c,\ Im\zeta=0\,,\ \text{on the draft plate}\,) \end{aligned} \tag{3.13}$$

where c $(0<c<1)$ is an undetermined real constant.

On the free surface, $\zeta=\exp(i\chi)$ $(0\le\chi\le\pi)$, the position $z=x+iy$ in the physical space can be expressed, by (3.9), as

$$x = -\frac{I(\chi)}{J(\pi)}\,, \quad y=-\frac{J(\chi)}{J(\pi)}\,, \tag{3.14}$$

$$I(\chi) = \int_0^{\chi} Rl(\frac{1}{w})\frac{\sin(\chi)}{(1+\cos(\chi))}d\chi, \tag{3.15}$$

$$J(\chi) = \int_0^{\chi} Im(\frac{1}{w})\frac{\sin(\chi)}{(1+\cos(\chi))}d\chi, \tag{3.16}$$

$$J(\pi) = \frac{\pi}{H}. \tag{3.17}$$

where $Rl(.)$ and $Im(.)$ stand for the real and imaginary part of $(.)$. The last equation (3.17) represents the result of applying the condition that $y(\chi)\to -1$ as $\chi\to\pi$ along the free surface towards the upstream infinity. After obtaining the solution to $w=w(\zeta)$, (3.17) is then a constraint condition by which the free stream water depth H is specified.

Finally, the dynamic condition on the free surface , (2.5) , is invoked by requiring that on $\zeta=\exp(i\chi)$,

$$w\overline{w}\ +y(\chi)=0, \quad (0\le\chi\le\pi)\,.$$

or, by (3.14)

$$w\overline{w} = \frac{J(\chi)}{J(\pi)}, \tag{3.18}$$

where $J(\chi)$ is given by (3.16) .

The problem remaining to be solved is to determine an explicit expression for $w(\zeta)$ which can facilitate the final stage of analysis and numerical computaion of the solution. As will be shown in the following chapter, this expression for $w(\chi)$ consists of two parts , $w(\zeta) = w_o(\zeta)\ w_c(\zeta)$, where $w_o(\zeta)$ is singular with known branch points at the stagnation point and at the bow-draft corner such that the kinematic conditions on the solid boundaries are satisfied whereas the unknown complimentary part, $w_c(\zeta)$, can assume the form of a power series. With this expression of $w(\zeta)$, it can be determined from (3.18) as a nonlinear integral equation for $w(\zeta)$, under the constraint condition (3.17) for subscribing the water depth.

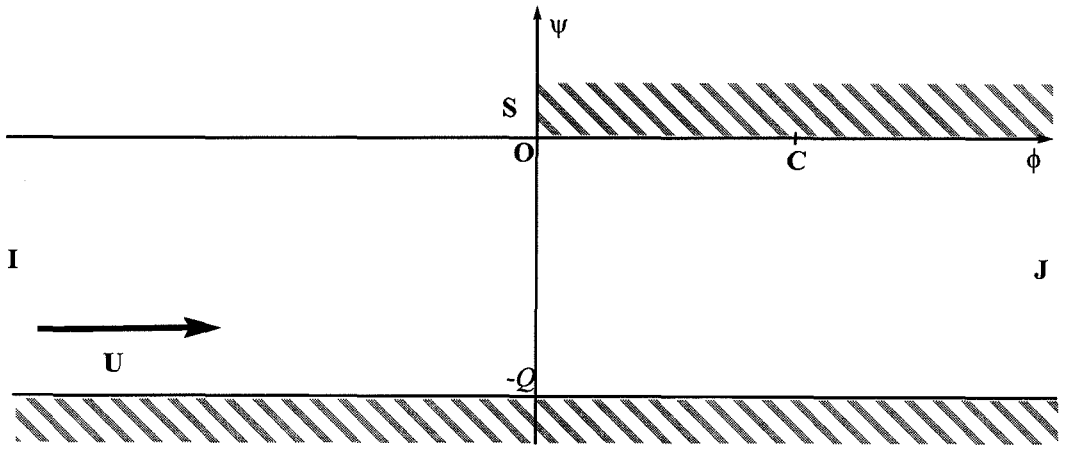

Figure 3.1: The flow field in f-plane

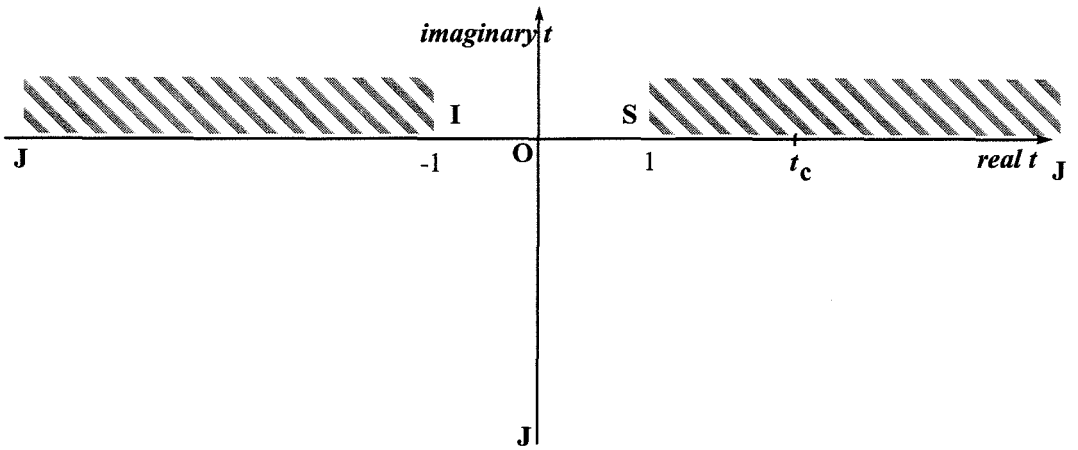

Figure 3.2: The flow field in t-plane

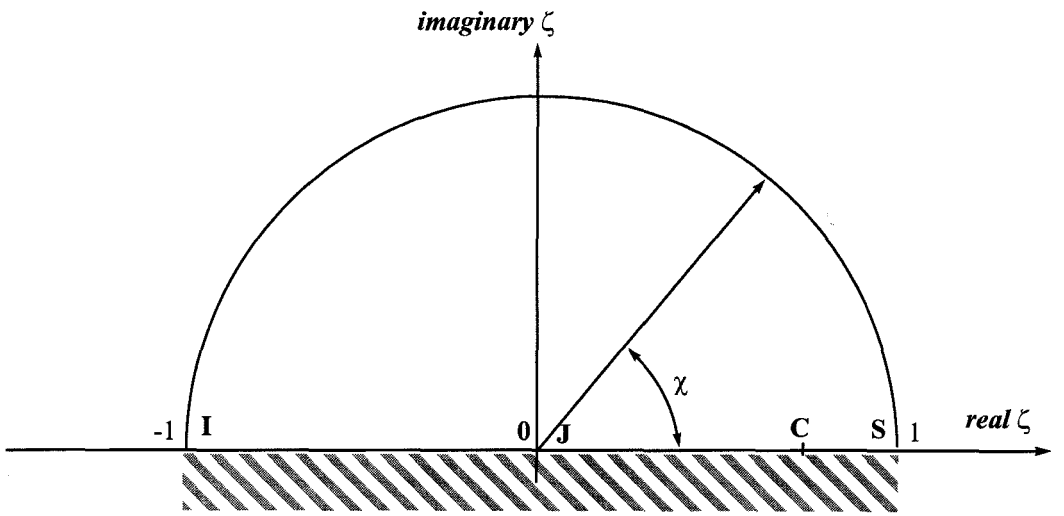

Figure 3.3: The flow field in ζ-plane

Chapter 4 The Local Corner Flows

In this chapter, we are concerned with local flows in a neighborhood of the stagnation point and about the bow-draft corner. These local solutions are needed to determine the value of the wedge angle β and the range of the incidence angle α of the bow plate that will assure existence of smooth and accurate solutions.

The corner flow about the stagnation point is assumed to be locally a flow within a wedge bounded on one side by the wetted bow plate and on the other by the free surface, as illustrated in Figure 4.1 . This simplification of the local flow is ideal to avoid unnecessary details without affecting the essential features of the result that is required.

Our local flow analysis shows that the wedge angle β between the free surface and the front bow plate must be equal to $120°$ for the incidence angle $0° < \alpha < 60°$. For $\alpha > 60°$, no local flow solution can exist. If there is no local solution for the given set of parameters, no global solutions can exist either. If there is a local solution, the global solution still remains to be sought.

The higher order singularities of these local solutions in a neighborhood of the stagnation point and of the free stream at upstream infinity are found to have branch-point singularities of irrational orders. By understanding their structures, we can incorporate them into the full solution.

4.1 Corner Flow Solution

The same conformal mappings as described in the last chapter can still be used. Near the stagnation point at $t = 1$, the lowest order local solution of $w(t)$ for the corner flow is given by

$$w_1(t) = qe^{-i\theta} = e^{-(\tau+i\theta)} = A(t-1)^{(1-\hat{\beta})}e^{i\alpha}, \quad (\hat{\beta} = \beta/\pi \ , \ \text{as} \ t \ \rightarrow \ 1), \tag{4.1}$$

where A is a real positive constant. In the neighborhood of $t = 1$, for $|t-1| << 1$, this $w_1(t)$ gives $\theta = -\alpha$ on the plate for $t > 1$ and $\theta = \pi - \beta - \alpha$ on the free surface for $t < 1$, which satisfies the kinematic condition on the bow plate.

On the free surface and near the stagnation point, $0 < 1 - t << 1$, we have

$$q = A(1-t)^{(1-\hat{\beta})} \ , \quad \theta = \pi - \beta - \alpha. \tag{4.2}$$

To satisfy the dynamic condition on the free surface, we differentiate the Bernoulli equation (2.14) with respect to ϕ , giving

$$2q^2\frac{\partial q}{\partial \phi} + \sin\theta = 0, \tag{4.3}$$

because $\partial y/\partial\phi = v/q^2 = (\sin\theta)/q$. In terms of t , we have,

$$2q^2\frac{\partial q}{\partial t} = -\frac{H}{\pi}\frac{\sin\theta}{t+1}, \tag{4.4}$$

since $Q = HU = H$. Substituting (4.2) in (4.4) yields

$$2A^3(1-\hat{\beta})(1-t)^{(2-3\hat{\beta})} = \frac{H}{2\pi}\sin(\pi - \beta - \alpha), \quad (0 < 1 - t << 1). \tag{4.5}$$

This is satisfied for all t in this limiting range if

$$\hat{\beta} = \frac{2}{3}, \text{ or } \beta = \hat{\beta}\pi = \frac{2}{3}\pi \ (= 120°) \tag{4.6}$$

$$\text{and } A^3 = \frac{3H}{4\pi}\sin(\frac{\pi}{3} - \alpha). \tag{4.7}$$

Thus, the wedge angle β of the free surface flow at the stagnation point is determined to be $\beta = 2\pi/3 = 120°$. Since $A > 0$ as required by the local conformal mapping (4.1), (4.7) imposes an additional condition that the local solution can exist if

$$0 < \alpha < \frac{\pi}{3} \quad (\text{ or } 0 < \alpha < 60°), \tag{4.8}$$

in which the lower bound is clear on the physical ground for the bow to remain submerged. The conditions (4.6) and (4.8) together imply that the free surface approaches the stagnation point from below. In addition, we point out that (4.7) arises as a condition on the magnitude A of q defined in (4.2) .

The above analysis is for the lowest order local solution of $w(t)$ near the stagnation point at $t = 1$. By extending our analysis to higher orders, the local solution of $w(t)$ for the corner flow can be rewritten as

$$\begin{aligned} w_1(t) &= qe^{-i\theta} = e^{-(\tau+i\theta)} \\ &= (t-1)^{(1-\hat{\beta})}e^{i\alpha}\ \exp\Big(\sum_{m=0}^{m=\infty}\sum_{n=0}^{n=\infty} a_{mn}\ (t-1)^{m\mu+n}\Big), \\ &\qquad (\hat{\beta} = \beta/\pi\ = \frac{2}{3},\ \text{as } t\ \to\ 1), \end{aligned} \tag{4.9}$$

where the coefficients a_{mn} and the index μ are all real, and $\hat{\beta} = 2/3$, as just determined. Moreover, the first coefficient a_{00} is related to A defined earlier by $\exp(a_{00}) = A$. Such choice of $w_1(t)$, including series expansions of analytic ($m =$

0) and branch point types ($m \geq 0$) , is necessary for the local solution to be matched at all orders, as will be shown presently.

In the neighborhood of $t = 1$, for $|t-1| << 1$, this new $w_1(t)$ gives $\theta = -\alpha$ on the plate for t real, $t > 1$. On the free surface and near the stagnation point, t real , $0 < 1 - t << 1$, we have

$$\begin{aligned} q &= (1-t)^{(1-\hat{\beta})} \exp\left\{ \sum_{m=0}^{m=\infty} \sum_{n=0}^{n=\infty} a_{mn} \, (1-t)^{m\mu+n} \, \cos\left[\pi(m\mu+n)\right] \right\}, \\ \theta &= \frac{1}{3}\pi - \alpha + \sum_{m=0}^{m=\infty} \sum_{n=0}^{n=\infty} a_{mn} \, (1-t)^{m\mu+n} \, \sin\left[\pi(m\mu+n)\right]. \end{aligned} \tag{4.10}$$

Thus, both q and θ have higher order terms that will be shown below as needed to satisfy (4.4) and to make the free stream turn smoothly as it approaches the stagnation point. In the limit $t \to 1$, $\theta = \pi - \beta - \alpha$ on the free surface, as has been determined in (4.6) with $\beta = 2\pi/3$.

Substituting (4.10) into the Bernoulli equation (4.4) gives , to the lowest order ($m = 0$ and $n = 0$), exactly (4.5) which we already obtained earlier. The matching of the next order in μ (i. e. , $m = 1$ and $n = 0$) yields

$$3\,(1+\mu)\tan\left(\frac{1}{3}\pi - \alpha\right) = \tan(\pi\mu). \tag{4.11}$$

The above expression is a transcendent equation and have infinite number of irrational roots, $0 < \mu_1 < \mu_2 < \ldots$. In Figure 4.2 , the smallest root μ_1 lies in the range $0 < \mu_1 < 0.5$ depending on the value of α . Here we note that $\mu \to 0$ as $\alpha \to \pi/3$ $(= 60°)$. The coefficient a_{10} can not be determined but can remain arbitrary in this matching.

For higher-order matchings based on (4.4), we will only state our results with-

out showing the details of derivation. To the higher-orders matching of (4.4), we found that all of the coefficients a_{mn}'s for $m \neq 0$ can be expressed in terms of the coefficient a_{10} which remains arbitrary. In addition, a_{0n}'s for $n \geq 1$ can be determined explicitly. The determination of the arbitrary coefficient a_{10} must come from the full solution that satisfies the constraint condition (3.17) as an integral equation.

4.2 Negative Pressure on the Bow Plate

By examining the pressure on the bow plate, we will discover more specific new features due to variations in the angle of incidence α . For the lowest order analysis of local corner flow, we take the bow plate and the free surface to be two flat sides, both semi-infinite in length, following the same ideal simplification adapted above. First, we examine the pressure on the bow plate. If the pressure is positive on the whole plate, the solution is physically feasible and admissible, so that the plate will exert an onward normal force on the fluid while delivering a positive amount of mechanical work on the fluid (in the absolute frame with the fluid at rest at infinity, of course) . However, if the pressure vanishes or becomes negative on the whole plate, the fluid would require a suction appropriately distributed over the plate to remain in contact with the bow plate. But the suction would do a negative work, corresponding to extracting flow energy from the fluid and so the present potential flow solution may not exist by itself. It will be shown below that the situation of having negative pressure on the entire wedge plate actually arises for the incidence angle $\alpha < 30°$. This exact solution for the wedge flow will be used to characterize the local flow near the stagnation point for further interpretation

and discussion of the final results pertaining to the present problem.

To find the pressure $p(x, y)$ on the semi-infinite bow plate, we apply Bernoulli's equation in the t- plane (2.13)

$$q^2 + p(x, y) + y = 0, \tag{4.12}$$

after setting the ambient pressure $p_0 = 0$.

From (3.3), the position z is given by

$$z = x + iy = \int_1^t \frac{1}{w(t)} \frac{df}{dt} dt, \tag{4.13}$$

in which we may substitute $f = (H/\pi)(t - 1)$ in (4.13) to convert the local stagnation corner flow to the ideal case of the entire (unbounded) wedge flow.

In order to find y on the bow plate, we take t real and $t > 1$. Substituting w from (4.1) into (4.13), we obtain

$$z = \frac{H}{2\pi A\hat{\beta}} (t - 1)^{\hat{\beta}} e^{-i\alpha}.$$

Hence, on the wedge plate, with t real, $t > 1$, and with $\hat{\beta} = 2/3$, we have

$$x + iy = \frac{3H}{4\pi A} (t - 1)^{\frac{2}{3}} (\cos\alpha - i \sin\alpha). \tag{4.14}$$

To find the pressure on the bow plate, we first obtain from (4.1) and (4.6) that on the wedge plate,

$$q^2 = A^2 (t - 1)^{2\ (1-\hat{\beta})} = A^2 (t - 1)^{\frac{2}{3}}, \quad (t > 1). \tag{4.15}$$

Substituting (4.14, 4.15) into Bernoulli's equation (4.12) gives

$$p = -y - q^2 = \frac{3H}{4\pi A}(t-1)^{(\frac{2}{3})}(\sin(\alpha) - \frac{4\pi A^3}{3H}). \tag{4.16}$$

By invoking (4.7), we then find that

$$p = \frac{3H}{4\pi A}(t-1)^{(\frac{2}{3})}(\sin(\alpha) - \sin(\frac{\pi}{3} - \alpha)), \tag{4.17}$$

which is simply

$$p = \frac{3^{\frac{3}{2}}H}{4\pi A}(t-1)^{\frac{2}{3}}\ \sin(\alpha - \frac{\pi}{6})\ , \quad (t \geq 1). \tag{4.18}$$

This exact solution for the unbounded wedge flow shows that the pressure on the bow plate is positive for $30° < \alpha < 60°$, vanishes over the entire plate at $\alpha = 30°$ and becomes negative for $\alpha < 30°$. This implies that the fluid would leave the bow plate by itself unless an appropriate suction is applied over the plate to prevent this from happening. For the global flow past the bow-draft plate now being considered, this means there should exist a negative pressure region in a neighborhood of the stagnation point and the fluid in this region would separate from the bow plate unless an adequate suction distribution could be provided over the bow plate. Even if adequate suction could be furnished as required, it remains to be determined whether the solution may exist for the assumed flow with $\alpha < 30°$. In this respect, we take note that under the said circumstance, predicted region of negative pressure are found indeed to occur in the numerical results as will be shown later.

In summary, we shall regard the range of incidence $30° < \alpha < 60°$ as a sound basis to proceed with our analysis of the solution intended. Nevertheless we will

still pursue successful resolutions of the problem for the range of $0° < \alpha < 30°$.

4.3 The Bow-draft Corner Flow

The local flow in a neighborhood of the corner joining the bow and draft plates at $t = t_c$ can be readily represented by the conformal mapping

$$w(t) = qe^{-i\theta} = e^{-(\tau+i\theta)} = \left(\frac{t-t_c}{1+t_c}\right)^{-\hat{\alpha}} G_1(t) \ , \quad (\hat{\alpha} = \alpha/\pi \ , \ \text{as } t \ \rightarrow \ t_c), \quad (4.19)$$

where $G_1(t)$ is an analytic function, regular in a neighborhood of $t = t_c$ and real positive on the real t-axis so that $\theta = 0$ for t real, $> t_c$, and $\theta = -\alpha$ for t real, $t < t_c$, thereby satisfying the kinematic condition on the bow-draft plate across the corner.

4.4 The Asymptotic Behavior of the Free Stream

Here, we shall first assume the radiation condition to hold: that no gravity waves can propagate upstream to infinity. Physically this assumption is based on the reasoning that the group velocity of the gravity waves, regarded as the velocity of propagating wave energy, is less than their phase velocity which is taken to hold, even under the nonlinear effects due to finite curvature of the free surface. Under this assumption, the asymptotic behavior of the free stream at upstream infinity can be conveniently investigated in a neighborhood of $t = -1$ in the lower half t-plane.

To proceed, we note that (i) $\theta = -\arg w = 0$ on the bottom plate (t real,

$t < -1$) , and (ii) $w \rightarrow 1$ (implying $\omega = \log(1/w) = \tau + i\theta \rightarrow 0$) as $t \rightarrow -1$ from below (in the lower half t-plane) . For the asymptotic free stream, we may therefore assume

$$\omega = \tau + i\theta = \sum_{m=1}^{m=\infty} b_m \left((t+1)e^{i\pi}\right)^{m\nu}, \quad (\text{ as } t \rightarrow -1), \tag{4.20}$$

where ν is real, > 0 , yet to be determined, and b_m's are real constants. This form of ω is found appropriate for describing the asymptotic free stream to be matched to any order.

On the bottom plate, $\theta = 0$ for t real, $t < -1$. On the free surface of the free stream, we have,

$$\tau + i\theta = \sum_{m=1}^{m=\infty} b_m (t+1)^{m\nu} (\cos m\nu\pi + i \sin m\nu\pi), \quad (t \text{ real}, 0 < 1+t << 1). \tag{4.21}$$

Substituting (4.21) into the Bernoulli equation (4.4) , which can also be written as

$$e^{-3\tau} \frac{\partial \tau}{\partial t} = \frac{H}{2\,\pi} \frac{\sin\theta}{(t+1)}, \quad (H/2 = gH/U^2 = F_h^{-2}), \tag{4.22}$$

we find , to leading term with $m = 1$,

$$\begin{aligned} e^{-3\tau} \frac{\partial \tau}{\partial t} &= b_1 \nu (t+1)^{\nu-1} \cos \nu\pi, \\ \frac{H}{2\,\pi} \frac{\sin\theta}{t+1} &= \frac{b_1 H}{2\,\pi} (t+1)^{\nu-1} \sin \nu\pi, \end{aligned}$$

whence

$$\nu\pi F_h^2 = \tan(\nu\pi), \tag{4.23}$$

where $F_h = U/\sqrt{gH} = \sqrt{2/H}$. Equation (4.23) has infinite number of roots, $0 < \nu_1 < \nu_2 < \ldots$, all irrational in general. Their values have two branches, according as the free stream is subcritical ($F_h < 1$) or supercritical ($F_h > 1$) . For the smallest root ν_1 , Figure 4.3 shows that $1 < \nu_1 < 1.5$ in the subcritical regime ($F_h < 1$) , and $0 < \nu_1 < 0.5$ in the supercritical regime ($F_h > 1$) .

For the higher-orders ($m = 2, 3, 4, \ldots$) matching of the Bernoulli equation (4.22), we found that all the b_m's can eventually be expressed in terms of b_1 . We notice that the asymptotic free stream depends only on the first coefficient b_1 , which is arbitrary, and which can be evaluated from the full solution satisfying the constraint condition (3.17) .

As commented previously, we shall only consider the subcritical regime (with $0 < F_h < 0.5$ say) in this work, leaving the other regime for further studies in view of the distinct features that the unsteady effects may be outstanding in the transcritical range and hydraulic jumps are generally manifest in front of the bow in the supercritical regime. Although we shall devote our subsequent effort only to the subcritical case of this bow wave problem, we should nevertheless note that for analyzing the solitary wave of maximum height (hence with a cornered crest subtending an angle of 120°) , the flow is supercritical throughout.

In passing, we note that equation (4.21)-(4.23) imply that, to the leading order,

$$w = u - iv = 1 + Ae^{\nu\pi x}, \quad (\text{ as } x \to -\infty), \tag{4.24}$$

A being a real constant, which shows an exponential decay of w towards the upstream uniform flow with the rate of an irrational index.

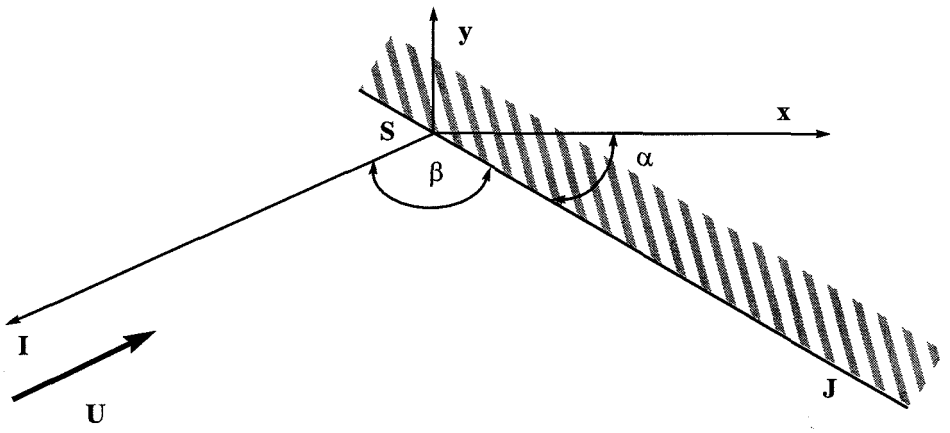

Figure 4.1: Local flow in z-plane near the stagnation point

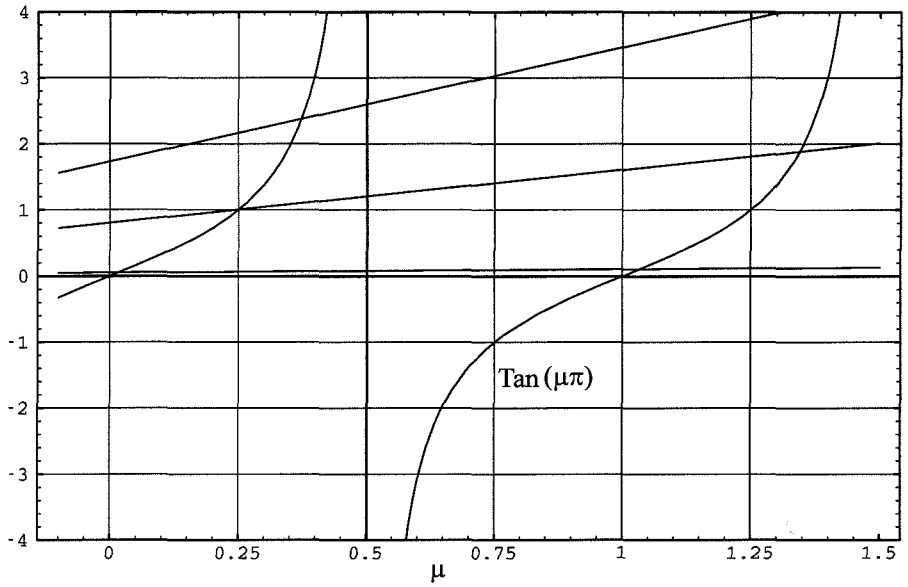

Figure 4.2: Plots of $\tan(\pi\mu)$ and $3\,(1+\mu)\tan(\frac{1}{3}\pi-\alpha)$ are shown for three values of α as a function of μ . The lower, middle and upper straight lines correspond to $\alpha = 59°$, $45°$ and $30°$ respectively. The two curves in the figure correspond to $\tan(\mu\pi)$. The roots of (4.11) are located at the intersections of the straight lines with the curves in the figure.

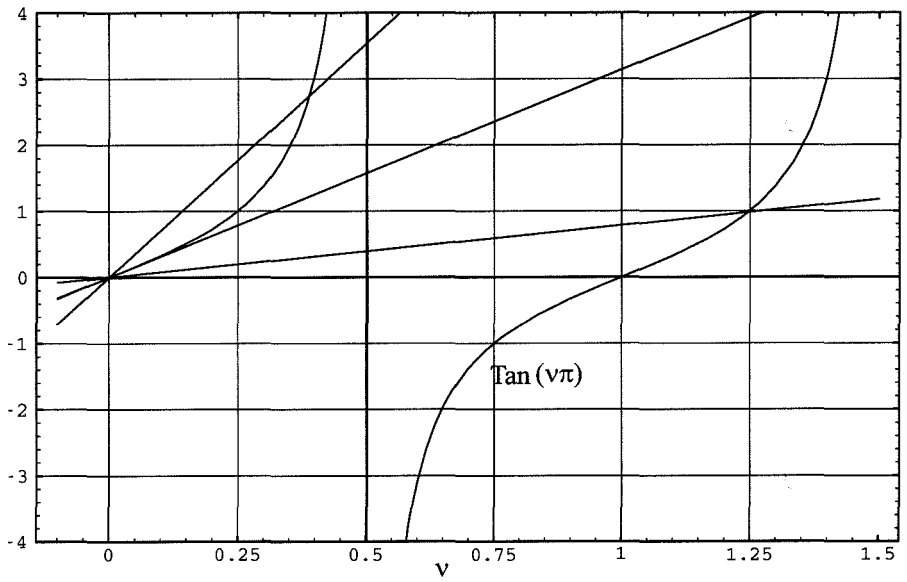

Figure 4.3: Plots of $\tan(\nu\pi)$ and $\nu\pi F_h^2$ are shown for three values of F_h as functions of ν . The lower straight line for $F_h = 0.5$ corresponds to the subcritical case, the middle straight line for $F_h = 1.0$ corresponds to the transcritical case and the upper straight line for $F_h = 1.5$ corresponds to the supercritical case. The two curves in the figure correspond to $\tan(\nu\pi)$. The intersections of the straight lines with the curves in the figure give the roots of (4.23) .

Chapter 5 The Velocity Field

Having determined the branch-point singularities of the velocity field at all the corner flows in the previous chapter, we proceed to construct the solution for the hodograph variable by synthesis and incorporation of the asymptotic corner flows into the full solution.

5.1 Synthesis of the Complex Velocity

For simplicity and convenience, it is desirable to solve for the complex velocity w in terms of the ζ-plane given by (3.5) . Based on the asymptotic representations of w at the various corners of the flow field obtained in the previous chapter, we assume

$$w(\zeta) = qe^{-i\theta} = w_o(\zeta)\, w_c(\zeta)\,, \tag{5.1}$$

$$w_o(\zeta) = q_o e^{-i\theta_o} = \left(\frac{1-\zeta}{2}\right)^{\frac{2}{3}} \left(\frac{(c-\zeta)(1-c\zeta)}{(1+c)^2}\right)^{-\frac{\alpha}{\pi}}\,, \tag{5.2}$$

where $\zeta = 1$ corresponds to the stagnation point at $f = 0$ (and $z = 0$) , $\zeta = c$ $(0 < c < 1)$ is the image point of $t = t_c$ (> 1) , and the multi-valued function $w_o(\zeta)$ is rendered unique by introducing a branch cut from $\zeta = 1$ to $\zeta = \infty$ outside the upper half circle $|\zeta| < 1$, $Im\zeta \geq 0$ (e.g. in the lower half ζ-plane) and another branch cut from $\zeta = c$ to $\zeta = 1/c$ just below the real ζ-axis . Here, w_o is the asymptotic representation of $w(\zeta)$ in the neighborhood of the stagnation corner at $\zeta = 1$ and of w near the bow-draft plate corner at $\zeta = c$, whilst w_c stands for the

complementary part of $w(\zeta)$ such that $w(\zeta)$ satisfies all the boundary conditions and the correct asymptotic properties of the stagnation corner flow and those of the free stream as have been identified. More precisely, $w_o(\zeta)$ has the following properties

$$\begin{aligned} (a)\quad \theta_o &= 0 \quad (-1 < \zeta < c < 1, \quad \text{on the draft and bottom plates}), \\ (b)\quad \theta_o &= -\alpha \quad (c < \zeta < 1, \quad \text{on the inclined bow plate}). \end{aligned} \tag{5.3}$$

On the unit circle, $|\zeta| = 1$, $\zeta = \exp(i\chi)$, we have for $0 < \chi < \pi$,

$$w_o(e^{i\chi}) = \left(\sin\frac{\chi}{2}\right)^{\frac{2}{3}} \left(1 - \frac{4c}{(1+c)^2}\cos^2\frac{\chi}{2}\right)^{-\frac{\alpha}{\pi}} \exp\left(i\,(\frac{1}{3} - \frac{\alpha}{\pi})\,(\chi - \pi)\right). \tag{5.4}$$

Hence,

$$(c)\quad \theta_o = \frac{\pi}{3} - \alpha \quad (\text{as } \chi \to 0, \quad \text{towards stagnation along the free surface}).$$

In addition, near $\zeta = -1$, the free stream value of $w_o(\zeta)$ assumes the asymptotic expansion:

$$\begin{aligned} (d)\quad w_o(\zeta) &= 1 + (\frac{\alpha}{\pi} - \frac{1}{3})(\zeta + 1) + \\ &\left(\frac{1}{2}\frac{\alpha}{\pi}(\frac{\alpha}{\pi} - \frac{2c}{(1+c)^2} + \frac{1}{3}) - \frac{1}{36}\right)(\zeta+1)^2 + O\,|\zeta+1|^3 \ . \end{aligned}$$

In contrast, we have shown that for the free stream velocity field, the boundary conditions imposed on the bottom plate and the free surface jointly require $w(\zeta)$ to take the asymptotic expansion (4.20) , or in terms of ζ to the leading term,

$$w(\zeta) = 1 + B\,(\zeta+1)^{2\nu} + o\,|\zeta+1|^{2\nu} \quad (\text{as } \zeta \to -1), \tag{5.5}$$

where B is a real constant, and use has been made of the relation (3.5) , which gives $(t+1)e^{i\pi} = (\zeta+1)^2/2$ as $\zeta \rightarrow -1$. For the subcritical regime now under consideration, we have already shown (see the part below 4.20) that with ν being the smallest root of (4.23) ,

$$2 < 2\nu < 3 \quad (\text{for } F_h < 1). \tag{5.6}$$

In this case ($F_h < 1$), we therefore have $w_o(\zeta) \rightarrow 1$ at a rate of $O(|\zeta+1|)$, which is lower in order than that of $w(\zeta)$ as indicated by (5.5)-(5.6). These distinct rates of $w(\zeta)$ and $w_o(\zeta)$ in their limits tending to unity will have to be reconciled through the construction of the complementary part $w_c(\zeta)$.

Guided by the above analysis, we may summarize the requirements that must be satisfied by $w_c(\zeta) = q_c \exp(-i\theta_c)$:

$$\begin{aligned}
&(a) \quad w_c(\zeta) \text{ is analytic, bounded in } |\zeta| \leq 1, \quad Im\zeta \geq 0, \\
&(b) \quad \theta_c = 0 \quad (-1 < \zeta < 1, \quad Im\zeta = 0), \\
&(c) \quad w_c(\zeta) \rightarrow 1 \text{ as } \zeta \rightarrow -1 \text{ such that (5.5) be satisfied.}
\end{aligned} \tag{5.7}$$

These conditions imply that $w_c(\zeta)$ is analytic, regular everywhere in $|\zeta| \leq 1, Im\zeta \geq 0$, except possibly at $\zeta = -1$ and $\zeta = 1$ where it may have branch points such that $w_c(\zeta)$ is purely real on the real ζ-axis, $-1 < \zeta < 1$. Hence, $w_o(\zeta)$ may be continued analytically into the entire unit circle $|\zeta| \leq 1$ by the symmetry of $w_c(\zeta)$ about the real ζ-axis.

Therefore, by invoking conditions (a) - (c) of (5.7) , we assume the following

form

$$\frac{1}{w_c(\zeta)} = 1 + b_1(\zeta+1) + b_2(\zeta+1)^2 + (\frac{\zeta+1}{2})^{2\nu} \sum_{m=0}^{m=\infty} \sum_{n=0}^{n=\infty} a_{mn} \, (\frac{1-\zeta}{2})^{2m\mu} \, \zeta^n, \tag{5.8}$$

with

$$b_1 = \frac{\alpha}{\pi} - \frac{1}{3},$$
$$b_2 = \frac{1}{2}\frac{\alpha}{\pi}(\frac{\alpha}{\pi} - \frac{2c}{(1+c)^2} + \frac{1}{3}) - \frac{1}{36},$$

where the unknown coefficients a_{mn}'s are all real so that $w_c(\zeta)$ is purely real for real ζ . With the coefficients b_1 and b_2 so assigned, the asymptotic behavior (5.5) for $w(\zeta)$ at upstream infinity as well as the local properties of $w(\zeta)$ near the stagnation point can then be satisfied by (5.8). The irrational exponent μ is taken to be the smallest root of (4.11) , $0 < \mu < 0.5$. On the unit circle, $|\zeta| = 1$, $\zeta = \exp(i\chi)$, we have for $0 < \chi < \pi$,

$$Rl\left(\frac{1}{w_c}\right) = 1 + (2b_1 + 4b_2\cos\chi)\cos^2\frac{\chi}{2} + (\cos\frac{\chi}{2})^{2\nu} \sum_{m=0}^{m=\infty} \sum_{n=0}^{n=\infty} a_{mn}(\sin\frac{\chi}{2})^{2m\mu} \cos\left[(m\mu + n + \nu)\chi + \pi m\mu\right],$$
$$Im\left(\frac{1}{w_c}\right) = b_1\sin\chi + 4b_2\cos^2\frac{\chi}{2}\sin\chi + (\cos\frac{\chi}{2})^{2\nu} \sum_{m=0}^{m=\infty} \sum_{n=0}^{n=\infty} a_{mn}(\sin\frac{\chi}{2})^{2m\mu} \sin\left[(m\mu + n + \nu)\chi + \pi m\mu\right], \tag{5.9}$$

where Rl and Im stand for the real and imaginary parts of $1/w_c$, respectively.

Now, to satisfy the corner flow solution (4.6) , we have $w(\zeta)$ from (5.4) and

(5.8) so that as $\zeta \rightarrow 1$, (m = 0)

$$w(\zeta) = \frac{\left(\frac{1-\zeta}{2}\right)^{\frac{2}{3}} \left(\frac{(1-c)^2}{(1+c)^2}\right)^{-\frac{\alpha}{\pi}} e^{i\alpha}}{1 + 2b_1 + 4b_2 + \sum_{n=0}^{n=\infty} a_{0n}}, \tag{5.10}$$

or in the t-plane as $t \rightarrow 1$, we have for $w(t)$ to the leading order

$$w(t) = A(t-1)^{\frac{1}{3}} e^{i\alpha}, \tag{5.11}$$

hence from (5.10) and (5.11)

$$A = \frac{\left(\frac{1}{2}\right)^{\frac{1}{3}} \left(\frac{(1-c)^2}{(1+c)^2}\right)^{-\frac{\alpha}{\pi}}}{1 + 2b_1 + 4b_2 + \sum_{n=0}^{n=\infty} a_{0n}}. \tag{5.12}$$

Substituting A from (5.12) into (4.7) and rearranging the terms, we obtain the second constraint condition,

$$\begin{aligned} \sum_{n=0}^{n=\infty} a_{0n} \; + \; S = 0, & \qquad (5.13) \\ S \; = \; 1 + 2b_1 + 4b_2 - \left[\frac{(1-c)^2}{(1+c)^2}\right]^{-\frac{\alpha}{\pi}} & \left[\frac{3H}{2\pi} \sin\left(\frac{\pi}{3} - \alpha\right)\right]^{-\frac{1}{3}}. \end{aligned}$$

The dynamic boundary condition on the free surface in a neighborhood very close to the stagnation point ($|\zeta| = 1$ and $\zeta \rightarrow 1$) is satisfied exactly by (5.13) .

Finally , the downstream condition (2.2) requiring that as $\zeta \rightarrow 0$, $w(0) = U_1 = H/(H-d)$ can be deduced from (5.1) (5.2) and (5.8) to give.

$$\left[\frac{1}{2}\right]^{\frac{2}{3}} \left(\frac{c}{(1+c)^2}\right)^{-\frac{\alpha}{\pi}} = \frac{H}{H-d}\left[1 + b_1 + b_2 + \left(\frac{1}{2}\right)^{2\nu} \sum_{m=0}^{m=\infty} a_{m0}\left(\frac{1}{2}\right)^{2m\mu}\right]. \tag{5.14}$$

This condition (5.14) can be conveniently used to assign values to the draft d as a

priori. This completes the formal analysis of the solution for $w(\zeta)$.

The foregoing analysis now leads to the solution in terms of the integral equations (3.14) and (3.18) from which the unknown coefficients a_{mn}'s and c can be determined in terms of the parameters ($\alpha, H = 2/F_h^2, d$) by numerical methods, as will be presented in the following chapters.

Chapter 6 Numerical Method

In this chapter, we describe the mumerical formulation which we used to solve the integral equations (3.14)-(3.18) and the second constraint condition (4.7).

By substituting the complex velocity $w(\zeta)$ from (5.4) and (5.9) in the Bernoulli equation (3.15), we obtain

$$w\overline{w} = w_c\overline{w_c}\ H(\chi) = \frac{J(\chi)}{J(\pi)}, \tag{6.1}$$

$$\text{where}\ \ H(\chi) = (\sin\frac{\chi}{2})^{\frac{4}{3}}\left[1 - \frac{4c}{(1+c)^2}\cos^2\frac{\chi}{2}\right]^{-\frac{2\alpha}{\pi}}, \tag{6.2}$$

and,

$$\frac{1}{w_c}\left(\overline{\frac{1}{w_c}}\right) = Rl\left(\frac{1}{w_c}\right)^2 + Im\left(\frac{1}{w_c}\right)^2. \tag{6.3}$$

The real and imaginary parts of $1/w_c$ can be found from (5.9) .

To put the Bernoulli equation into a convinent form , we multiply both sides of the Bernoulli equation (6.1) with $J(\pi)\ \frac{1}{w_c}\left(\overline{\frac{1}{w_c}}\right)$,

$$J(\pi)\ H(\chi) = J(\chi)\ \frac{1}{w_c}\left(\overline{\frac{1}{w_c}}\right). \tag{6.4}$$

Such multiplication can be taken because both $J(\pi)$ and $\frac{1}{w_c}\left(\overline{\frac{1}{w_c}}\right)$ are not equal to zero. From (3.17), $J(\pi)$ never equals to zero since H is finite. From our intuition, the flow enters with a finite speed at the upstream infinite, and its speed decreases to zero as it approaches the stagnation point. Hence, w_c never becomes singular anywhere on the free surface.

For convinent, the first constraint condition (3.17) can be written

$$J(\pi) - \frac{\pi}{H} = 0, \tag{6.5}$$

where H is the dimensionless water depth at the upstream infinity and it does not relate to the function $H(\chi)$.

Our problem has now been reduced to finding the a_{mn}'s that satisfies both Bernoulli's equation (6.4) and two constraint conditions (6.5, 5.13) on the free surface.

6.1 Minimization

We select the minimization of error method to satisfy those equations optimally over the whole interval on the free surface. On the free surface, we define $F(\chi, a_{mn})$ as the difference between the left-hand side and right-hand side of the Bernoulli equation (6.4), the local error to be minimized. Similarly, let $G(a_i)$ and $K(a_i)$ be errors of the first and second constraint conditions respectively (6.5, 5.13) .

$$F(\chi, a_{mn}) = J(\pi)\, H(\chi) - J(\chi)\, \frac{1}{w_c} \left(\overline{\frac{1}{w_c}}\right) \tag{6.6}$$

$$G(a_{mn}) = J(\pi) - \frac{\pi}{H}, \tag{6.7}$$

$$K(a_{0n}) = \sum_{n=0}^{n=\infty} a_{0n} + S, \tag{6.8}$$

where both indexes m and n range from 0 to ∞ . We defined a total error $E(a_{mn})$, which is a positive quantity, as

$$E(a_{mn}) = \int_0^{\pi} F(\chi, a_{mn})^2 d\chi. \tag{6.9}$$

Since $E(a_{mn}), G(a_{mn})$ and $K(a_{mn})$ are functions of only the coefficients a_{mn}'s but not χ , we can treat a_{mn} as independent variables. Our problem is now transformed into the minimization of $E(a_{mn})$ with two constraint conditions $G(a_{mn}) = 0$ and $K(a_{0n}) = 0$.

6.2 Lagrange's Multiplier Method

To solve the problem exactly, an infinite number of modes a_{mn}'s are required, in theory. In particular, however, we solve those equations (6.6)-(6.9) with sufficiently large number of modes a_{mn}'s while expect that such truncation errors will be limited within certain small bound.

We use the method of Lagrange's multiplier to find the minimum of the total error $E(a_{mn})$ (6.9) under the two constraint conditions (6.7) and (6.8) , for which we employ two Lagrange's multipliers λ_1 and λ_2 corresponding to (6.7) and (6.8) .

A new function M , including the total error $E(a_{mn})$ and the two constraint equations, is defined as:

$$M(a_{mn}, \lambda_1, \lambda_2) = E(a_{mn}) - \lambda_1 \, G(a_{mn}) - \lambda_2 \, K(a_{0n}), \tag{6.10}$$

where the indices m and n range from 0 to $(M-1)$ and 0 to $(N-1)$, respectively. The total number of a_{mn}'s is $M \times N$. By including λ_1 and λ_2, there are $M \times N + 2$ independent variables in the function M .

To minimize the function M , the partial derivatives with respect to the

independent variables a_{mn}'s, λ_1 and λ_2 are set to zero,

$$\begin{aligned}
\frac{\partial M(a_{mn},\lambda_1,\lambda_2)}{\partial a_{mn}} &= \frac{\partial E(\chi,a_{mn})}{\partial a_{mn}} - \lambda_1\frac{\partial G(a_{mn})}{\partial a_{mn}} - \lambda_2\frac{\partial K(a_{0n})}{\partial a_{mn}} \\
&= 0, \quad (M\times N \text{ equations}) \qquad (6.11)\\
\frac{\partial M(a_{mn})}{\partial \lambda_1} &= -G(a_i) = 0. \quad (1 \text{ equation}) \qquad (6.12)\\
\frac{\partial M(a_{mn})}{\partial \lambda_2} &= -K(a_i) = 0. \quad (1 \text{ equation}) \qquad (6.13)
\end{aligned}$$

The explicit form of the last set of equations will be given later. We shall solve $M \times N + 2$ equations (6.11)-(6.13) for the $M \times N + 2$ unknowns by Newton's method.

6.3 Newton's Method

Since the set of equations (6.11)-(6.13) is already linear in terms of λ_1 and λ_2 but nonlinear in a_{mn}'s, the idea is to linearize the set of non-linear equations in terms of some previous known values of $a_{mn,0}$'s . For each a_{mn} , let a_{mn} be represented by the sum of two parts, $a_{mn} = a_{mn,0} + \Delta a_{mn}$ or with a change of dummy index to jk, $a_{jk} = a_{jk,0} + \Delta a_{jk}$. We then substitute a_{jk}'s into the set of equations and linearize the set, with Δa_{jk} considered as being small with respect to $a_{jk,0}$.

Next, applying linearization to $\partial E/\partial a_{nm}$, G and K , we take the partial derivatives with respect to the independent variables a_{jk} ,

$$\begin{aligned}
\frac{\partial E}{\partial a_{mn}} &= \left(\frac{\partial E}{\partial a_{mn}}\right)_0 + \Delta a_{jk}\left(\frac{\partial^2 E}{\partial a_{mn}\partial a_{jk}}\right)_0, \quad (M\times N \text{ equations}) \qquad (6.14)\\
G &= G_0 + \Delta a_{jk}\left(\frac{\partial G}{\partial a_{jk}}\right)_0, \quad (1 \text{ equation}) \qquad (6.15)
\end{aligned}$$

$$K = K_0 + \Delta a_{jk} \left(\frac{\partial K}{\partial a_{jk}} \right)_0, \quad \text{(1 equation)} \tag{6.16}$$

where j and k is summed from 0 to $(M-1)$ and 0 to $(N-1)$, respectively, in the above equations. Those functions with subscript $_0$ contain the independent variables $a_{mn,0}$'s or $a_{jk,0}$'s .

We substitute the expressions (6.14)-(6.16) into the set of equations (6.11)-(6.13) ,

$$\begin{aligned} \frac{\partial M}{\partial a_{mn}} &= \left(\frac{\partial E}{\partial a_{mn}} \right)_0 + \Delta a_{jk} \left(\frac{\partial^2 E}{\partial a_{mn} \partial a_{jk}} \right)_0 - \lambda_1 \left(\frac{\partial G}{\partial a_{mn}} \right)_0 - \lambda_2 \left(\frac{\partial K}{\partial a_{mn}} \right)_0 \\ &= 0, \quad (M \times N \text{ equations}) \end{aligned} \tag{6.17}$$

$$\frac{\partial M}{\partial \lambda_1} = -G_0 - \Delta a_{jk} \left(\frac{\partial G}{\partial a_{jk}} \right)_0 = 0, \quad \text{(1 equation)} \tag{6.18}$$

$$\frac{\partial M}{\partial \lambda_2} = -K_0 - \Delta a_{jk} \left(\frac{\partial K}{\partial a_{jk}} \right)_0 = 0, \quad \text{(1 equation)} \tag{6.19}$$

where $\partial G/\partial a_{mn}$, $\partial G/\partial a_{jk}$, $\partial K/\partial a_{mn}$ and $\partial K/\partial a_{jk}$ involve only $a_{mn,0}$ or $a_{jk,0}$ as constants, not a function of a_{mn} , a_{jk}, λ_1 and λ_2 .

In the matrix form, we rewrite (6.17)-(6.19) ,

$$\begin{pmatrix} \frac{\partial^2 E}{\partial a_{00} \partial a_{00}} & \cdots & \frac{\partial^2 E}{\partial a_{00} \partial a_R} & -\frac{\partial G}{\partial a_{00}} & -\frac{\partial k}{\partial a_{00}} \\ \frac{\partial^2 E}{\partial a_{01} \partial a_{00}} & \cdots & \frac{\partial^2 E}{\partial a_{01} \partial a_R} & -\frac{\partial G}{\partial a_{01}} & -\frac{\partial k}{\partial a_{01}} \\ \vdots & \ddots & \vdots & \vdots & \vdots \\ \frac{\partial^2 E}{\partial a_R \partial a_{00}} & \cdots & \frac{\partial^2 E}{\partial a_R \partial a_R} & -\frac{\partial G}{\partial a_R} & -\frac{\partial K}{\partial a_R} \\ -\frac{\partial G}{\partial a_{00}} & \cdots & -\frac{\partial G}{\partial a_R} & 0 & 0 \\ -\frac{\partial K}{\partial a_{00}} & \cdots & -\frac{\partial K}{\partial a_R} & 0 & 0 \end{pmatrix} \begin{pmatrix} \Delta a_{00} \\ \Delta a_{01} \\ \vdots \\ \Delta a_R \\ \lambda_1 \\ \lambda_2 \end{pmatrix} = \begin{pmatrix} -\frac{\partial E}{\partial a_{00}} \\ -\frac{\partial E}{\partial a_{01}} \\ \vdots \\ -\frac{\partial E}{\partial a_R} \\ G \\ K \end{pmatrix}, \tag{6.20}$$

where the subscripts $_0$ are omitted in the matrix element and the index R represents $(M-1)(N-1)$. The linearized matrix equation (6.20) is solved iteratively by Newton's method.

Let l be the number of iteration. For the first iteration $(l=1)$, the elements of a^0_{jk} equals some known values. In Newton's method, the initial choice of a^0_{jk} is important in determining the convergence of the method. For the l iteration,

$$a^l_{jk} = a^{l-1}_{jk} + \Delta a^{l-1}_{jk}, \quad l > 0, \tag{6.21}$$

in which the new a^l_{jk} are updated at every iteration. In the theory, Δa^{l-1}_j approaches zero if the the scheme converges. However, in the numerical computation Δa^{l-1}_j would approach a certain small bound, because of the truncation error.

6.4 The Matrix Elements

The matrix equation (6.20) contains a square matrix on the left-hand side and a single column matrix on the right hand-side. We shall give details on calculating elements of those matrixes.

For the square matrix on the left hand side of (6.20) , its elements involve E, G, K, F (6.6-6.9) and their first or second derivatives with respect to the independent variables a_{mn}'s or a_{jk}'s or both.

In summary, we list elements of the square matrix:

(a) On the last row or the last column of the square matrix, elements yield

$$\frac{\partial K}{\partial a_{mn}} = 1 \quad \text{if} \quad m = 0\ , \tag{6.22}$$

$$\text{or else} \qquad = 0 \quad \text{if} \quad m \neq 0\ .$$

Each of matrix elements (6.22) equals to 0 or 1 since K depends linearly on a_{0n}'s.

(b) On the second row or column from the last, matrix elements give

$$\begin{aligned} \frac{\partial G}{\partial a_{mn}} &= \frac{\partial J(\pi)}{\partial a_{mn}} \\ &= \int_0^{\pi} (\cos\frac{\chi}{2})^{2\nu} (\sin\frac{\chi}{2})^{2m\mu} \sin\left((m\mu + n + \nu)\chi + \pi m\mu + \theta\right) \\ &\quad \left(1 - \frac{4c}{(1+c)^2}\cos^2\frac{\chi}{2}\right)^{\frac{\alpha}{\pi}} (\sin\frac{\chi}{2})^{\frac{1}{3}}\, d\chi, \end{aligned} \tag{6.23}$$

where $\theta = (1/3 - \alpha/\pi)\ (\pi - \chi)$, index m ranges from 0 to $(M-1)$ and index n ranges from 0 to $(N-1)$. Evaluating elements (6.23) requires one integration that must be done numerically.

(c) Matrix elements having the second derivatives with respect to a_{mn} and/or a_{jk} are

$$\frac{\partial^2 E}{\partial a_{mn}\partial a_{jk}} = \int_0^{\pi} 2 \left(F\frac{\partial^2 F}{\partial a_{mn}\partial a_{jk}} + \frac{\partial F}{\partial a_{mn}}\frac{\partial F}{\partial a_{jk}} \right) d\chi, \tag{6.24}$$

where F , $\partial F/\partial a_{mn}$, and $\partial^2 F/\partial a_{mn}\partial a_{jk}$ can be evaluated from (6.6) . We will not show them here. The final expression of $\partial^2 E/\partial a_{mn}\partial a_{jk}$ (6.24) is straightforward and will not be presented explicitly. The matrix elements (6.24) need two numerical integrations.

For the column matrix on the right hand side of (6.20) , its elements contain $\partial E/\partial a_{mn}$, G and K . The last two elements G and H have been given earlier. Matrix elements of $\partial E/\partial a_{mn}$ give

$$\frac{\partial E}{\partial a_{mn}} = \int_0^{\pi} 2\ F\ \frac{\partial F}{\partial a_{mn}}\, d\chi, \tag{6.25}$$

where F and $\partial F/\partial a_{mn}$ can be evaluated from (6.6) . The final expression of $\partial E/\partial a_{mn}$ will be curtailed here. Calculating (6.25) involves one numerical inte-

gration.

We shall set forth the details of solving the minimization matrix equation (6.20). First, we use Simpson's method to evaluate the elements on both sides of (6.20) requiring double or single integrations with respect to the independent variable χ . Next, the matrix equation is solved by the Gaussian elimination method. The unknown Δa_{jk}'s are calculated iteratively using Newton's method (6.21) .

Our forgoing numerical procedure solves the matrix equation (6.20) from which a_{mn}'s and d can be found in terms of the parameters ($\alpha, H = 2/F_h^2, c$).

6.5 Inverse Iterative Method

An inverse iterative method is used in which the unknowns a_{mn}'s and c can be determined in terms of the given parameters ($\alpha, H = 2/F_h^2, d$).

This inverse method uses the downstream condition (5.14) which we can re-express as

$$c = \frac{-(2-r) - \sqrt{(2-r)^2 - 4}}{2}, \tag{6.26}$$

where

$$r = \left(\frac{2^{\frac{2}{3}} H}{H-d} (1 + b_1 + b_2 + (\frac{1}{2})^{2\nu} \sum_{m=0}^{m=\infty} a_{m0} (\frac{1}{2})^{2m\mu}) \right)^{\frac{\pi}{\alpha}},$$

and r represents a temporary variable.

We summarize the inverse iterative method as follows:

(a) An initial guess c_0 first be given. We usually take a value of c from some previously solved problem with slightly different parameters.

(b) By using the procedure given in the last section, we solve a_{mn}'s in terms of ($\alpha, H = 2/F_h^2, c$).

(c) From the downstream condition (5.14), c can be calculated in terms of the original parameters ($\alpha, H = 2/F_h^2, d$) and the temporary a_{m0}'s from step (b) .

(d) We repeat the steps (b) and (c) until c and a_{mn}'s converge to the solutions with certain pre-specified tolerance.

6.6 Free Surface and Bow Plates

Once we have determined a_{jk}'s and c , we proceed to compute the free surface shape , draft depth and the drag acting on the bow plate. The free surface shape gives the overall pattern of the flow. The bow draft depth and drag assure the accuracy of our numerical solutions, upon comparison the numerical result for the drag with another theorectical equivalence which is exact.

On the free surface, the position x and y given in (3.14) can be rewritten as a function of χ ,

$$x = -\frac{I(\chi)}{J(\pi)}, \quad y = -\frac{J(\chi)}{J(\pi)}, \tag{6.27}$$

$$J(\chi) = \int_0^{\chi} Y(\chi) \left(1 - \frac{4c}{(1+c)^2}\cos^2\frac{\chi}{2}\right)^{\frac{\alpha}{\pi}} \frac{(\sin\frac{\chi}{2})^{\frac{1}{3}}}{(\cos\frac{\chi}{2})} d\chi, \tag{6.28}$$

$$\begin{aligned} \text{and} \quad Y(\chi) &= Im\left(\frac{1}{w_c}\right)\cos\theta + Rl\left(\frac{1}{w_c}\right)\sin\theta \\ &= Y_0(\chi) + \sum_{m=0}^{m=\infty}\sum_{n=0}^{n=\infty} a_{mn} Y_{mn}(\chi), \end{aligned}$$

$$\text{where } Y_0(\chi) = \sin\theta + 2b_1 \sin\theta \cos^2\frac{\chi}{2} + 4b_2 \cos^2\frac{\chi}{2} \sin(\chi+\theta),$$
$$Y_{mn}(\chi) = (\cos\frac{\chi}{2})^{2\nu}(\sin\frac{\chi}{2})^{2m\mu} \sin((m\mu+n+\nu)\chi + \pi m\mu + \theta),$$

with $\theta = (1/3 - \alpha/\pi)(\pi - \chi)$ from (5.4).

Similarly,

$$I(\chi) = \int_0^\chi X(\chi) \left(1 - \frac{4c}{(1+c)^2}\cos^2\frac{\chi}{2}\right)^{\frac{\alpha}{\pi}} \frac{(\sin\frac{\chi}{2})^{\frac{1}{3}}}{(\cos\frac{\chi}{2})} d\chi, \tag{6.29}$$

$$\text{and} \quad X(\chi) = Rl\left(\frac{1}{w_c}\right)\cos\theta - Im\left(\frac{1}{w_c}\right)\sin\theta$$
$$= X_0(\chi) + \sum_{m=0}^{m=\infty}\sum_{n=0}^{n=\infty} a_{mn} X_{mn}(\chi),$$

$$\text{where } X_0(\chi) = \cos\theta - b_1 \sin\chi \sin\theta + 2b_1 \cos\theta \cos^2\frac{\chi}{2} + 4b_2 \cos^2\frac{\chi}{2} \cos(\chi+\theta),$$
$$X_{mn}(\chi) = (\cos\frac{\chi}{2})^{2\nu}(\sin\frac{\chi}{2})^{2m\mu} \cos((m\mu+n+\nu)\chi + \pi m\mu + \theta).$$

In our numerical computation, we shall take the free surface shape as one of our main results. We will show it in the next chapter.

To check the accuracy of our solutions for a_{mn}'s and c , we use an inverse method to find the position x and y of the corner of the bow in the physical plane.

Substituting $1/w$ given by (5.2 , 5.8) into the expression z (3.8) on the front plate (ζ real and $c < \zeta < 1$) , we write the position of the corner,

$$z = x + iy = \frac{H}{\pi}\int_1^c \frac{(\zeta-1)}{w(\zeta)(\zeta+1)\zeta} d\zeta, \tag{6.30}$$
$$\text{with} \quad \frac{1}{w(\zeta)} = (\cos\alpha - i\sin\alpha)(\frac{1-\zeta}{2})^{-2/3}\left(\frac{(\zeta-c)(1-c\zeta)}{(1+c)^2}\right)^{\frac{\alpha}{\pi}}$$

$$\times(1+b_1(\zeta+1)+b_2(\zeta+1)^2$$
$$+(\frac{\zeta+1}{2})^{2\mu}\sum_{m=0}^{m=\infty}\sum_{n=0}^{n=\infty}a_{mn}\,(\frac{1-\zeta}{2})^{2mp}\,\zeta^n),$$

with the expressions for b_1 and b_2 given in (5.8) .

By comparing the last expression (6.30) with the exact position of the corner of the bow determined from the initial values prescribed on α and d, we can verify the accuracy of our solutions.

Another method to check the accuracy of our solutions is to compare the drag on the front plate computed in two different ways. The first way for calculating the drag D_t is by theoretically formula derived from the balance of the x momentum integral equation,

$$D_t = d\,(\frac{d}{2}+1-\frac{H}{H-d})\,. \tag{6.31}$$

The drag (6.31) does not depend on α but only on H and d . The entire contribution to the drag comes from the front plate only since the drag is in the horizontal direction. The lift on the front plate can be computed from the drag since the total force on the bow plate must be perpendicular to it. However, the lift on the horizontal draft plate may be unbounded due to the length of the bow is semi-infinite.

In the secod way, the drag can also be found from the horizontal component of the pressure p integrating over the front plate. The pressure p acting on the bow can be computed from Bernoulli's equation (2.13) ,

$$p=-y-w\overline{w}. \tag{6.32}$$

Inserting w given by (5.2, 5.8) and y of (6.30) into the above equation, pressures

on the inclined plate and the horizontal plate can be found separately. The drag D_n on the front plate becomes:

$$D_n = \int_{-(d+1)}^{0} p\, dy = \int_c^1 p(\zeta)\, \frac{\partial y}{\partial \zeta}\, d\zeta\ . \tag{6.33}$$

In the next chapter, we will give and compare the two drags, D_t and D_n (6.31, 6.33) , which should be exactly the same.

6.7 New Improvement in Accuracy

To gain greater accuracy, we put more points near the stagnation point where the maximum error is expected to occur. On the free surface, we introduce a new real variable σ to replace χ by the transformation,

$$\chi = \frac{\pi}{2}(1 - \cos\sigma). \tag{6.34}$$

From this transformation, the point $\chi = 0$ and $\chi = \pi$ are transformed into $\sigma = 0$ and $\sigma = \pi$ respectively. In addition, the total error is redefined to change the variable of integration from χ to σ :

$$E(a_{mn}) = \int_0^{\pi} F(\chi(\sigma), a_{mn})^2 d\sigma. \tag{6.35}$$

We also change $\partial E/\partial a_{mn}$ (6.25) and $\partial^2 F/\partial a_{mn}\partial a_{jk}$ (6.24) consistently into:

$$\frac{\partial E}{\partial a_{mn}} = \int_0^{\pi} 2\, F\, \frac{\partial F}{\partial a_{mn}}\, d\sigma, \tag{6.36}$$

$$\frac{\partial^2 E}{\partial a_{mn}\partial a_{jk}} = \int_0^{\pi} 2 \left(F \frac{\partial^2 F}{\partial a_{mn}\partial a_{jk}} + \frac{\partial F}{\partial a_{mn}}\, \frac{\partial F}{\partial a_{jk}} \right) d\sigma. \tag{6.37}$$

By substituting the transformation (6.34) into all expressions containing integrations, the matrix equation (6.20) is solved similarly as before. We discuss the result of this improvement in next chapter.

Chapter 7 Numerical Results

The numerical method given in the last chapter has been applied to computing our model equations (6.4, 6.5, 5.13) to provide free surface profiles and to verify our local analysis of the branch- point singularities of the velocity field at the stagnation point and at the upstream infinity.

In a typical case, the free surface shape is shown in Figure 7.1 and 7.2 with the parameters $\alpha = 45°$, $H = 100$ and $d = 17$. In those figures, the vertical axis represents the free surface height y , and the horizontal axis represents the horizontal distance x . The bow is located to the right of the free surface y . The stagnation point is located at the origin. In Figure 7.1 for the global view, both the bow and the free surface are shown. A zoomed in plot of the free surface profile y is given in Figure 7.2 , in which the bow (not shown) is located to the right of the free surface; it exhibits the free surface profile changes its shape. Figure 7.2 shows that the free surface falls off smoothly and monotonically to zero from the stagnation point ($x = 0$) to the upstream infinity ($x = -\infty$) .

In typical case, we use 341 evenly spaced grid points in the new coordinate σ transformed from the coordinate χ on the upper half plane of the unit semi-circle in the ζ-plane and use a total of 32 modes of the coefficients a_{mn}'s (including $a_{1\ 0}$, $a_{2\ 0}$ and $a_{0\ 0}$ ... $a_{0\ 29}$). This is sufficient to give accurate and converged numerical results to the 5th decimal-places (e. g. the free surface profiles).

Figure 7.3 shows the velocity slope angle θ of the velocity (u, v) on the free surface based on the set of the parameters of Figure 7.2. The curve of θ showing

smooth and monotonic falls off steeply in a neighborhood of the stagnation point from 15° to 4° over a distance less than $2h$ and then levels off from 4° to 0° at the upstream infinity. Such a pattern of θ in the figure implies that we correctly incorporate the singularities of multiple irrational orders at both the stagnation point ($x = 0$) and the upstream infinity ($x = \infty$) . More definite evidences will be shown below with the issue pertaining to the rate of convergence of the series.

Corresponding to Figure 7.2 , the pressure distribution p on the inclined flat plate and the horizontal semi-infinite draft plate is shown in Figure 7.4 . In the pressure graph, the vertical axis represents the pressure p on the front and the trailing horizontal draft plates of the bow, while the horizontal axis represents the horizontal distance x . We note that p on the inclined plate of the graph increases slowly from zero at the stagnation ($x = 0$) to a maximum positive value and then falls off steeply to $-\infty$ in a small neighborhood of the bow-draft corner at $x = 17$. In addition, p on the horizontal plate of the graph rises steeply in the neighborhood of the bow-draft corner from $-\infty$ to a positive value and then level off to a constant positive value at the down stream infinity ($x = \infty$) . Since this singular behavior of p at the bow-draft corner agrees to the prediction of our local bow-draft corner flow analysis in the earlier chapter, it further demonstrates the exactness of our numerical result.

7.1 Convergence and Accuracy of the Results

The object of this section is to indicate the convergence and the accuracy of our numerical results. We consider numerical solutions well-converged if the solutions do not change significantly within a certain tolerance as the numbers of grid points

and modes of a_{mn}'s increase in our numerical computation. For the maximum difference between the left-hand and the right-hand sides of the Bernoulli Equation (3.18) , we usually set the error rounded to be $< 10^{-4}$.

As shown in Figure 7.5 , we confirm the convergence of our solutions by using the same set of parameters as in Figure 7.2 with the exception when using different numbers of modes of a_{mn}'s. Figure 7.5 demonstrates that the free surface curves y having different numbers of modes of a_{mn}'s are located closely on the top of each other. Hence, the solution is already converged and the error due to the truncation of the higher order terms of the infinite series to a finite series is small and insignificant (with the tolerance of 0.0001) . In Figure 7.6 , we compare the solutions of 341 and 1361 grid points while keeping the other parameters same as in Figure 7.5 . The free surface curves y of the figure are almost identical to each other. We conclude that the convergence of our solution is excellent. However, if less tolerance of the solution is required, greater numbers of modes a_{mn}'s and grid points will be needed to achieve the convergence of the solution.

The accuracy of the solutions of the bow problem can be further scrutinized by comparing the two values of the drag obtained numerically and theoretically. Our theoretical work of the bow problem gives for the drag coefficient derived from the balance of the x momentum integral equation (6.31), the formula

$$D_t = d\,(\frac{d}{2} + 1 - \frac{H}{H-d})\,. \tag{7.1}$$

Alternatively, the drag can also be computed by numerically integrating the pres-

sure acting on the bow plate,

$$D_n = \int_{-(d+1)}^{0} p\, dy = \int_c^1 p(\zeta)\, \frac{\partial y}{\partial \zeta}\, d\zeta \,. \tag{7.2}$$

A comparison between the two values for the same drag (7.1, 7.2) has been made based on the same set of parameters used in Figure 7.2 ($\alpha = 45°$, $H = 100$, 32 modes of a_{mn}'s) . For the pressure integral, we used 10041 grid points on the inclined bow plate to evaluate the drag (7.2) . Two values of the drag on the bow are thus found to be 141.01807 (theoretically by 7.1) and 141.00881 (numerically by 7.2); they agree with each other up to the 5th significant digits, with an error of 0.01 . Thus, the accuracy of our result is well confirmed.

Having established the fast-convergent and accurate numerical method, we proceed to investigate how the shape of free surface will vary with different values of the three parameters: the incidence angle α , the bow draft depth d , and the upstream water depth H .

7.2 Variations in the Incidence Angle

We examine the effect due to variations in the incidence angle α on the free surface profile while keeping d and H constant (see Figure 7.7) .

In Figure 7.8 , three free-surface profile curves are shown for $\alpha = 55°$, $45°$, and $35°$ appearing from top to bottom with the same set of parameters $d = 17$ and $H = 100$. The top free surface profile for $\alpha = 55°$ takes the slowest rate to fall off to zero at infinity. The middle free surface profile for $\alpha = 45°$ falls off steeper than the top curve. The discrepancies of these two curves is located primarily within

a horizontal distance x of $100h$ from the stagnation point $x = 0$. The bottom free surface curve for $\alpha = 35°$ falls off to zero at the steepest rate and shows very slight oscillations. This could be associated with the branching of our local corner solutions at the stagnation point for α arounds $30°$.

In Figure 7.9, we present the surface profiles with the draft kept constant at $d = 17$ but with the water depth increased to $H = 200$. The three curves represent the numerical results for the free surface for $\alpha = 55$, 45, and $35°$, appearing from top to bottom in Figure 7.9 respectively. The top curve for the free surface profile for $\alpha = 55°$ falls off to zero at the lowest rate, whereas the bottom curve free surface for $\alpha = 35°$ falls off to zero at the highest rate. The discrepancies among these curves are occured mostly within 100 h upstream from the stagnation point $(x = 0)$.

The numerical results presented in Figure 7.10 are with the draft depth $d = 17$, the water depth $H = 50$, for the incidence angle $\alpha = 55$, 45, and $35°$ respectively. We note that the third sets of figures can be quantitatively differentiated to exhibit the effect due to variations in α , but qualitatively similar.

We next proceed to examine the effects on the free surface profile due to variations in the draft depth d and water depth H .

In Table 7.1 , we present a list of numerical data on the numerically-computed drag D_n acting on the bow and the theoretically- calculated drag D_t jointly with the free surface curves on these three figures (Figure 7.8, 7.9, 7.10). For each row, the values of α , d , H , Fr_d , Fr_h , the number of grid points , the number M of modes a_{m0}'s, the number N of modes a_{0n}'s, D_n , and D_t are given. By comparing D_n and D_t for each row, we can see that their values agree with each other to

at least four significant digits. Hence, D_n is accurate up to this limit. From the theoretical drag (7.1) , we note that the drag does not depend on the angle of incidence α . This implies that the discrepancies between the fall off rates of the free surface curves on each figure are not related to the drag because they have to vary in such a manner as to keep the drag unaffected.

7.3 Variations in the Draft Depth

We next investigate the effect due to the variations in the draft depth d on the free surface profile while keeping α and H fixed (see figure 7.11) .

The first figure of the second set (7.12) presents five curves, appearing from top to bottom, which represent the free surface profiles for the draft deph of 3, 9, 17, 40, and 70 ($Fr_d = 0.816, 0.471, 0.343, 0.224$, and 0.169). The parameters of the first figure include $\alpha = 45°$ and $H = 100$ $(Fr_h = 0.141)$. Starting from the largest draft depth of 70 , we can explore the effects of decreasing draft depth. The top free surface curve for $d = 70$ having the largest draft depth, takes the longest horizontal distance to fall off to zero, the middle curves decrease faster than the first one, in their orders, and the bottom curve falls off with the largest slope to zero. Clearly, it shows that the rate of decrement of the free surface is negatively correlated to the draft deph d . The curve of the smallest slope is associated with the largest draft depth d and vice versa.

The free surface shapes of the top two curves $(d = 40, 70)$ have only very small differences apart. This seems to suggest that the free surface shape changes slowly, approaching a limiting shape as the draft depth increases beyond 50 percent of the water depth. The reason is that the added inertial effect from increasing draft

depth does not effectively reach the free surface.

As the draft depth decreases to only $3h$, the bottom curve exhibits oscillations of finite amplitude which bring forth a new class of free-surface profile in contrast with that the monotonic shape as shown above.

To help explain how this breakdown takes place, we examine the pressure disribution over the front and horizontal plates of the bow. Corresponding to the fourth curve from the top for $d = 9$ in Figure 7.12, the pressure distribution on the plates is given in Figure 7.13 , which shows that the pressure on the front plate (in Figure 7.13) is almost all positive except for a very small negative region near the corner of the bow where the pressure becomes $-\infty$. The pressure distribution on the plates of the bow corresponding to the bottom curve for $d = 3$, is plotted against the horizontal distance x in Figure 7.14 . For comparison , the negative pressure region for $d = 3$ at the corner of the bow in Figure 7.14 is located closer to the stagnation point than the negative pressure region for $d = 9$ in Figure 7.13. In general, the importance of the presence of a negative pressure region in the neighborhood of the corner of the bow grows when the draft depth decreases. We believe strongly that this growing negative pressure region eventually causes the steady wavy profile to arise.

In the second and third figures of the second set, we show two additional combinations of α and H . In the second figure shown in Figure 7.15 , we set $\alpha = 45°$ and $H = 50$ ($Fr_h = 0.2$) while keeping d at 3, 9, 17, 21 and 25 . In the third figure (Figure 7.16) , we use $\alpha = 55°$ and $H = 200$ (draft length d of 3, 9, 17, 40 and 70). Similarly, there are five curves of the free surfaces shown in each figure. Since the patterns of the second and third figures are identical to the

pattern of the first figure in the second set, we do not give the details.

For all 15 free surface curves included in the three figures of the second set, their corresponding drags D_t and D_n are shown in Table 7.2 . For each horizontal row, we notice that D_t agrees very well with D_n . So, the accuracy of our numerical results are uniformly excellent. In general, for each figure of the second set, the drag D on the bow increases with increasing d . Physically , for a greater drag D, the inertial effect in an inner region near the stagnation point is greater because the bow pushes the fluid harder; thus, the free surface falls off slower.

To summarize, we note that if the solutions are monotonic and smooth, , the effects due to decreasing draft depth d are the following: the free surface falls off faster to zero, the magnitude of the drag D on the bow becomes smaller, and the importance of the negative pressure region at the corner of the bow grows.

7.4 Variations in the Water Depth

We now proceed to study the effects due to variations in water depth H on the free surface shape while keeping d and α constant, as depicted in Figure 7.17 . In this third set of results, three combinations of d and α are shown in three different figures.

In the first figure of the third set (Figure 7.18), $d = 17$ ($Fr_d = 0.343$) and $\alpha = 45°$, the free surface profiles are for $H = 35, 50, 100, 200$, and 400 ($Fr_h = 0.239, 0.2, 0.141, 0.1$, and 0.071). Since $Fr_h < 1$ and not close to unity for all the five curves, the free surface profiles are all smooth, monotonic, and well-converged. We note that the top curve ($H = 400$) falls off at the slowest rate to zero from the stagnation point to the upstream infinity and the bottom curve ($H = 50$) falls off

at the fastest rate to zero. The higher falling rate is associated with shallower water depth H and is due to a weaker inertial effect in the inner region near the stagnation point. The reason is that the total pressure on the flat bottom plate of the channel is the sum of two parts, one is being the static fluid pressure corresponding to the state when there is no flow, and the other part the excess pressure which does dynamically affect the flow. From the Bernoulli equation (2.13) ,

$$(\hat{u}^2 + \hat{v}^2) + \hat{p}(x, y) + \hat{y} = 0, \quad \text{in the flow domain,} \tag{7.3}$$

the magnitude of velocity squared can be related to the excess pressure. From the law of conservation of mass (2.2) and the Bernoulli equation (7.3) , the velocity U_1 (downstream infinity) at $+\infty$ must increase with decreasing the water depth H . Thus, the velocity on the flat bottom surface also must increase. Since the velocity increases on the bottom surface, by applying the Bernoulli equation, we see that the excess pressure will be smaller. Effectively, the bottom surface does not push the moving fluid as strongly as before; therefore, the free surface falls off faster.

Another important observation is that in Figure 7.18 , every free surface curve starting from the stagnation point decreases quickly first to a tail region in which the curve then falls off very slowly to zero at the upstream infinity. From the top curve of Figure 7.18, we observe that the free surface descends to a slowly sloping tail region at a distance of about $80h$ from the stagnation point. For greater water depth H , the tail region grows longer. This could be a primary reason for explaining the difficulties encountered in determining solution for $H = \infty$.

Similarly, we can show well-converged solutions for the second and third figures

of the third set. In the second figure (Figure 7.19) , five free surface curves are shown for the water depth $H = 35, 50, 100, 200, 400)$ together with $\alpha = 55°$ and $d = 17$. In the third figure, (Figure 7.20) , another group of five curves are given for the water depth $H = 35, 50, 100, 200, 400$, with $\alpha = 35°$ and $d = 17$. The patterns of the curves in the second and third figures are similar to the pattern in the first figure. The conclusion is the same for all three figures.

In Table 7.3 , we show D_t and D_n corresponding to all the free surface curves in the three figures of the third set. By comparing the drags D for the curves of each figure in the third set, we find that the drag D on the bow increases with increasing water depth H .

To obtain a monotonic well-converged solution, we prefer to keep the water depth H greater than $10h$ ($Fr_h < 0.4$). Otherwise, the solution will be oscillating or not convergent. In addition, as Fr_h approaches 1, we expect that there will be intrinsically unsteady waves generated moving upstream.

7.5 Pressure Variation Near $\alpha = 30°$

In this section, we further examine the free surface profile with the incidence angle α around 30° while keeping H and d fixed.

From our local flow analysis near the stagnation point, the angle of incidence α around 30° exhibits two distinct types of flow behavior. For the first type with $\alpha > 30°$, the fluid pressure increases from zero at stagnation and remains positive on the bow plate until the bow- draft corner is approached. For the second type with $\alpha < 30°$, a region of negative pressure exists adjacent to the stagnation point for $\alpha < 30°$. The presence of negative pressure appears to confirm the

expectation raised in Chapter 4 based on the free surface wedge flow. The criticality in the incidence angle of $\alpha = 30°$ associated with the negative pressure adjacent to the stagnation is thought to be responsible for giving rise to the conspicuous phenomenon of steady wave profile on the upstream side of the bow plate.

Next, we compare the results of our local flow analysis and numerical results. In Figure 7.21 , the free surface height is plotted against the horizontal distance x for the angle of incidence $\alpha = 35°$, $31°$, $27°$, and $22°$ with the water depth $H = 100$ and draft length $d = 17$. The top curve corresponds to $\alpha = 35°$. The second curve from the top represents $\alpha = 31°$ and shows small oscillations. The third and fourth curves ($27°$ and $22°$) from the top show large oscillations. Those oscillations have the same wavelength which is very nearly equal to the wavelength of the free waves in deep water, which is 4π in the present dimensionless form. Moreover, the amplitudes of the oscillations of the wavy free surface decrease to zero at a sufficiently large distance (more than 100 h) , a result which implies the waves are not radiating energy. Clearly, the results of these wavy surface represent a new type of flow solutions.

In Figure 7.22 , the pressures corresponding to the free surface curves of Figure 7.21 are presented in a neighborhood of the stagnation point on the inclined bow plate. For $\alpha = 31°$ and $35°$, the pressure distributions are positive in a neighborhood of the stagnation point and monotonically increasing downstream on the front bow plate . On the other hand, for $\alpha = 27°$, there exists a small negative pressure region next to the stagnation point on the front bow plate. As α decreases to $22°$, the negative pressure region increases in size. This negative pressure region for $\alpha < 30°$ is responsible for the changing of the solution and

agrees with our local flow analysis predictions.

In our observation, the solution bifurcates (from the smooth profile class to the wavy profile class) even before α decreases to 30° , since our analysis on the criteria with the negative pressure is only a local one. However, our computational results show a global solution. The draft depth d and water depth H modify our result from local analysis slightly . Nevertheless, the breakdown of the solution involving smooth profiles around $\alpha = 30^\circ$ seems to possess a sound validity.

If the flow should be reversed, we might first think that the oscillatory solution would be a good solution for steady gravity waves moving behind the bow. Since we have imposed the radiation condition of no outgoing waves to the upstream infinity, the oscillatory solution does in fact satisfy this condition. Thus, the wavy profile solution is ruled out to be a steady-wave solution for the reverse flow that radiates wave energy.

The drags D_t and D_n on the bow are shown in Table 7.4 , from which we observe the following: (1) the numerical and theoretical drags agree very well with each other, and (2) that the drags corresponding to different values of α also agree very closely.

In general, with other combinations of d and H , the branching of solution around $\alpha = 30^\circ$ is invariably found to manifest. To gain comprehension about the new phenomenon of the upstream wavy motion on water, more research will be required.

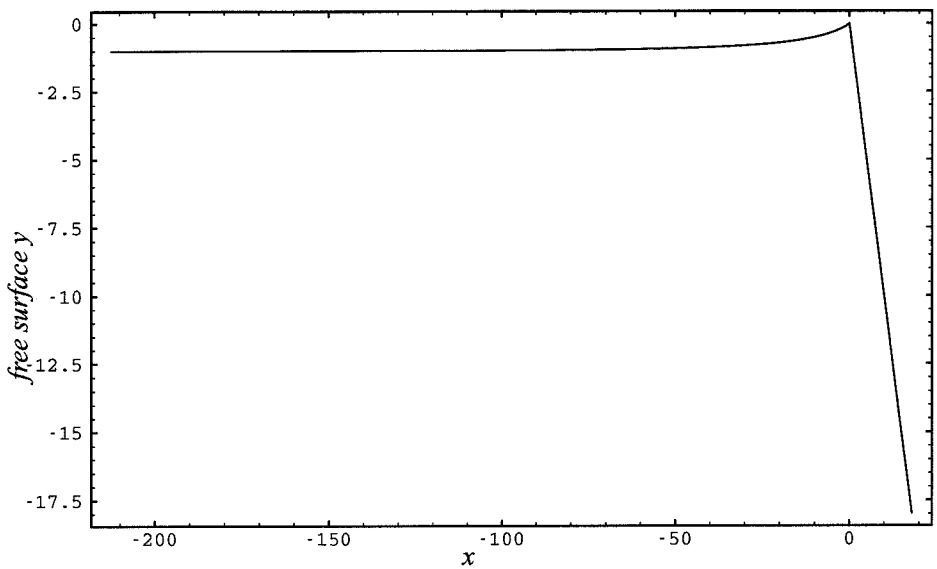

Figure 7.1: The profiles of Free surface and front bow plate for $\alpha = 45°$, $H = 100$, $d = 17$ with 2+30 modes of a_{mn}'s , 341 grid points.

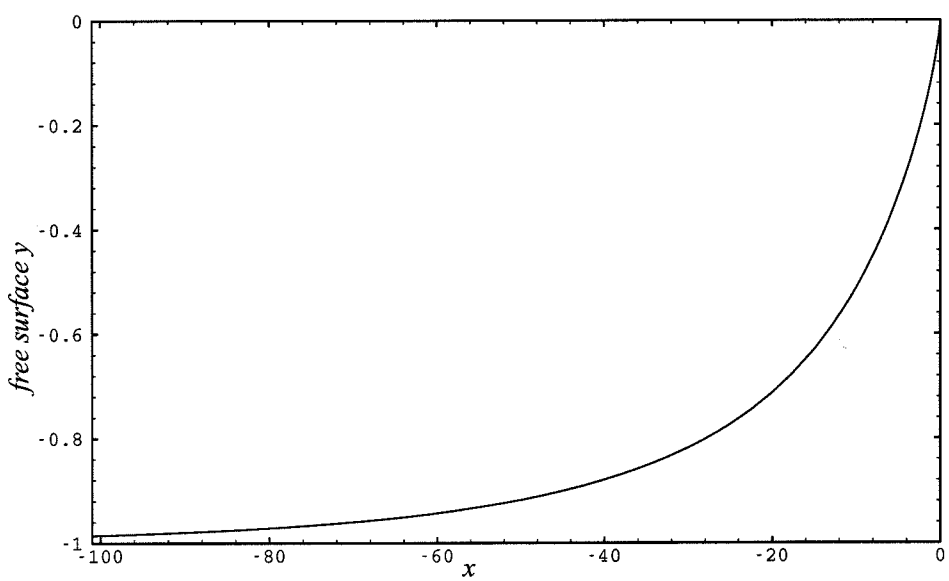

Figure 7.2: Magnified free surface profile with the maximum relative error of 0.000009 for $\alpha = 45°$, $H = 100$, $d = 17$ employing 2+30 modes of a_{mn}'s , 341 grid points.

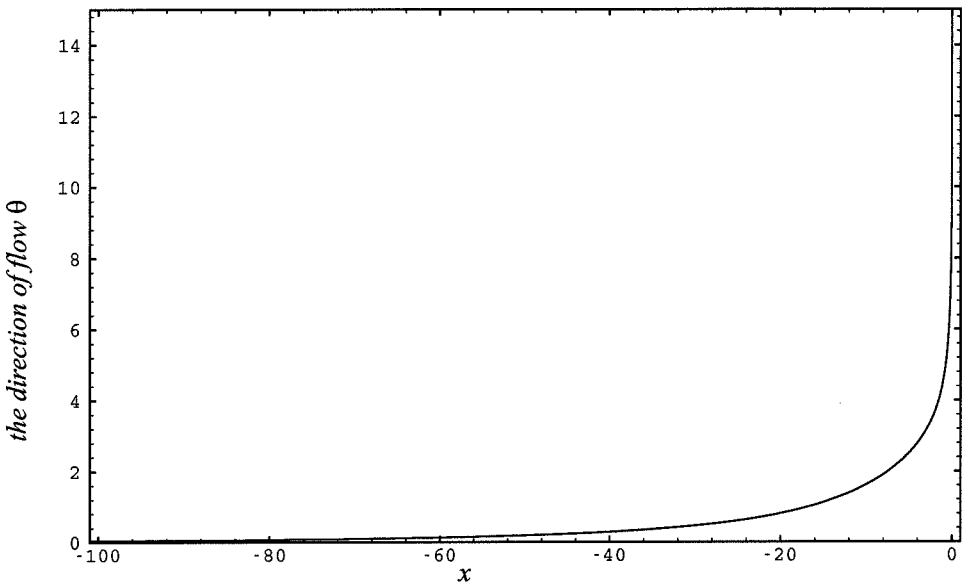

Figure 7.3: Velocity flow direction θ (degrees) on the free surface for $\alpha = 45°$, $H = 100$, $d = 17$ with 2+30 modes of a_{mn}'s , 341 grid points.

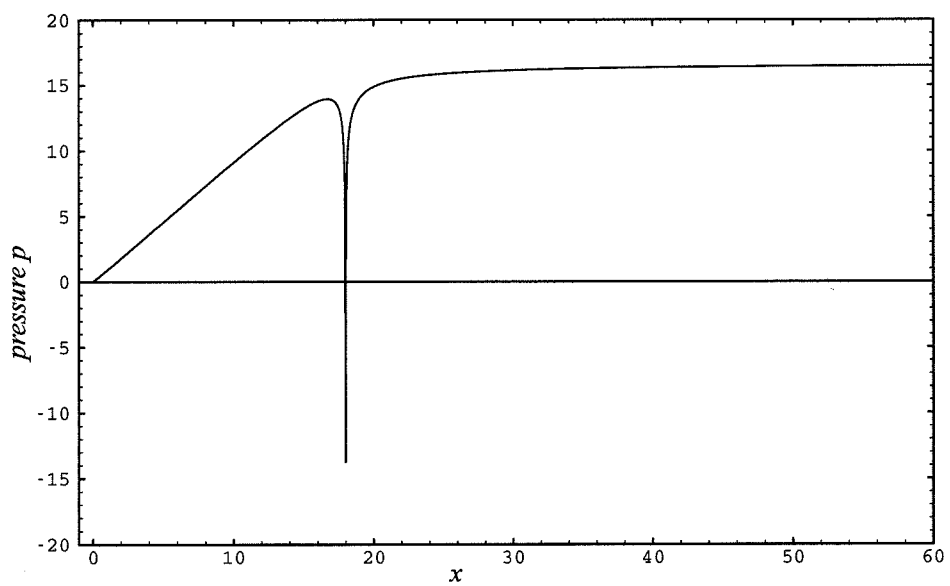

Figure 7.4: Pressure on the bow plate and horizontal draft plate for $\alpha = 45°$, $H = 100$, $d = 17$ with 2+30 modes of a's , 341 grid points.

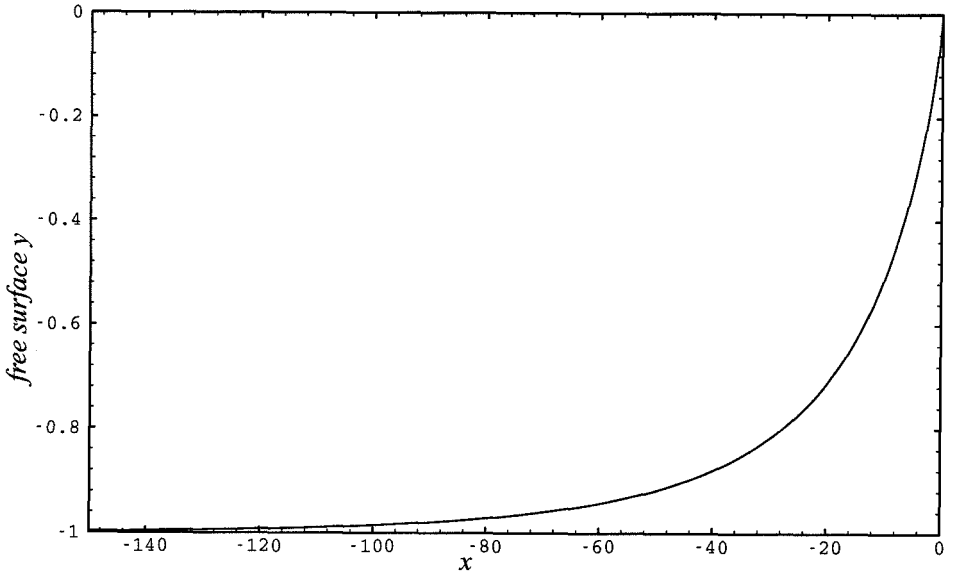

Figure 7.5: Comparison between the two results for the free surface profile obtained with 2+30 and 5+60 modes of a_{mn}'s for $\alpha = 45°$, $H = 100$, $d = 17$, using 341 grid points.

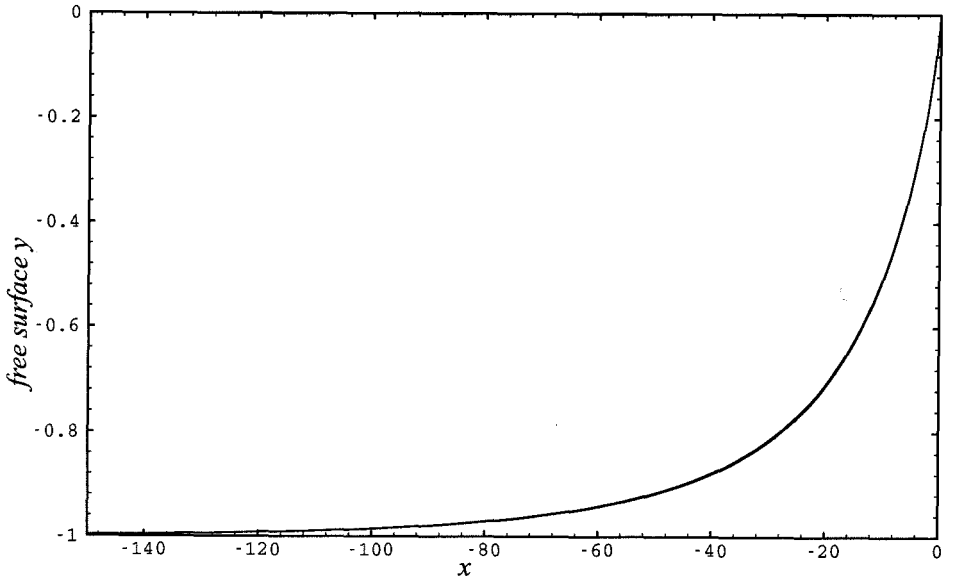

Figure 7.6: Comparison between the two results for the free surface profile obtained with 341 and 1361 grid points for $\alpha = 45°$, $H = 100$, $d = 17$, using 2+30 modes of a_{mn}'s.

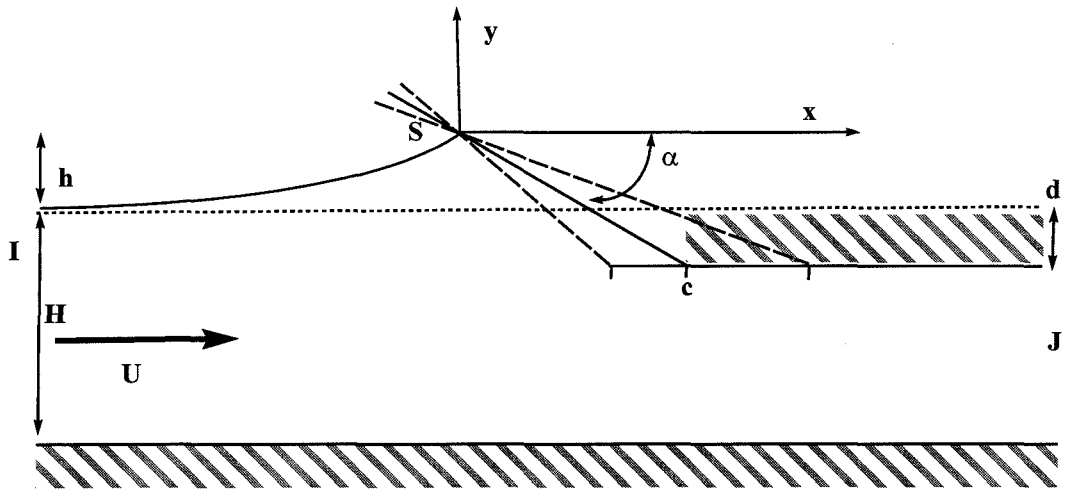

Figure 7.7: A sketch of the bow plate with variations in the incidence angle α .

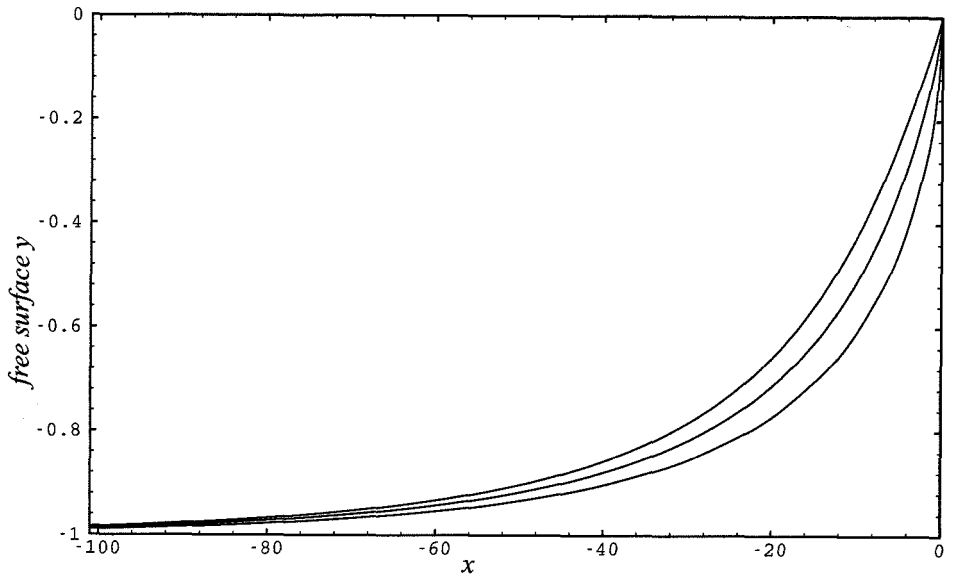

Figure 7.8: Variations of free-surface profile with varying the incidence angle for $\alpha = 55°$ (top), $45°, 35°$(bottom) , with $H = 100$, $d = 17$, using 2+30 or 4+30(top) modes of a_{mn}'s.

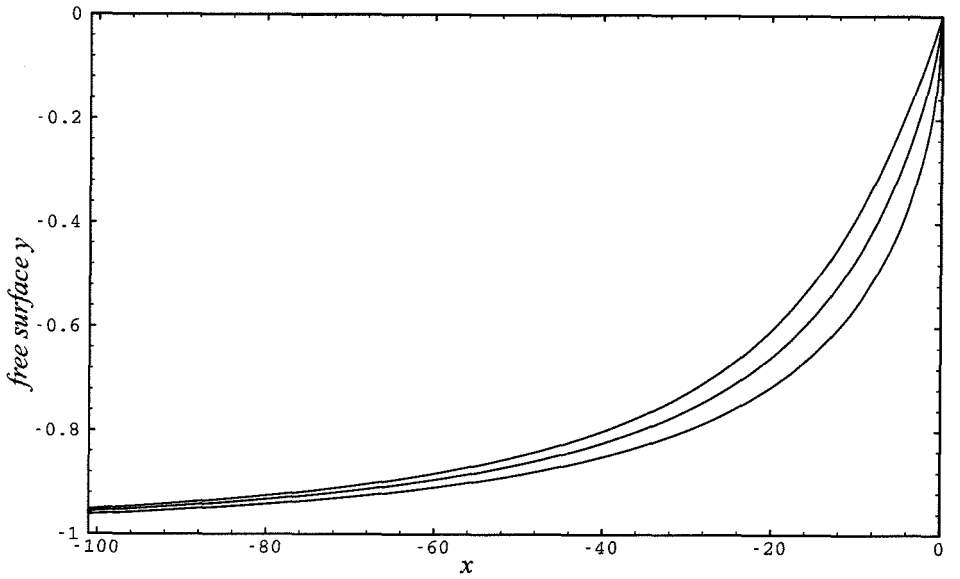

Figure 7.9: Variation of free-surface profile with varying the incidence angle for $\alpha = 55°$(top), $45°, 35°$(bottom), with $H = 200$, $d = 17$, using 2+30 or 4+30(top) modes of a_{mn}'s.

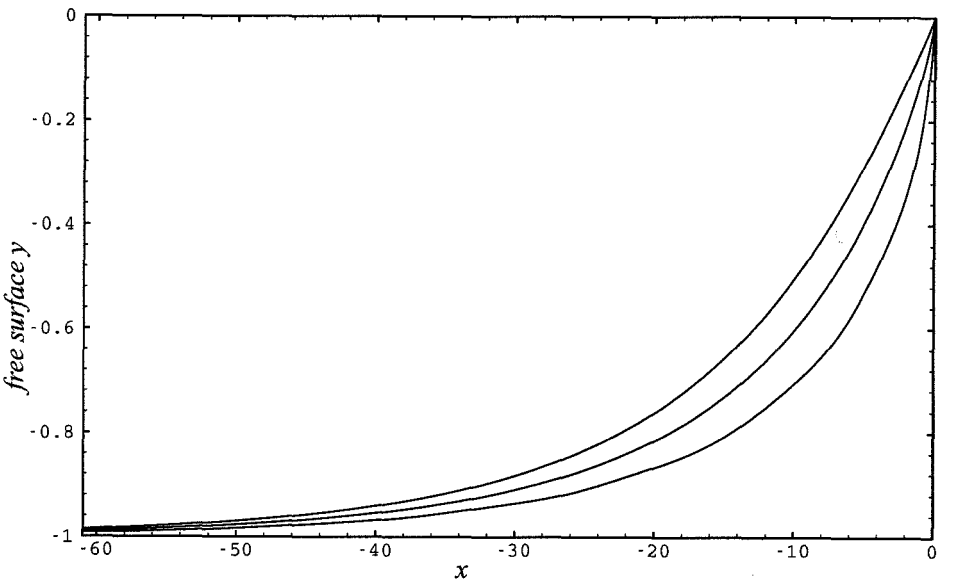

Figure 7.10: Variation of free-surface profile with varying the incidence angle for $\alpha = 55°$(top), $45°, 35°$(bottom), with $H = 50$, $d = 17$, using 2+30 or 4+30(top) modes of a_{mn}'s.

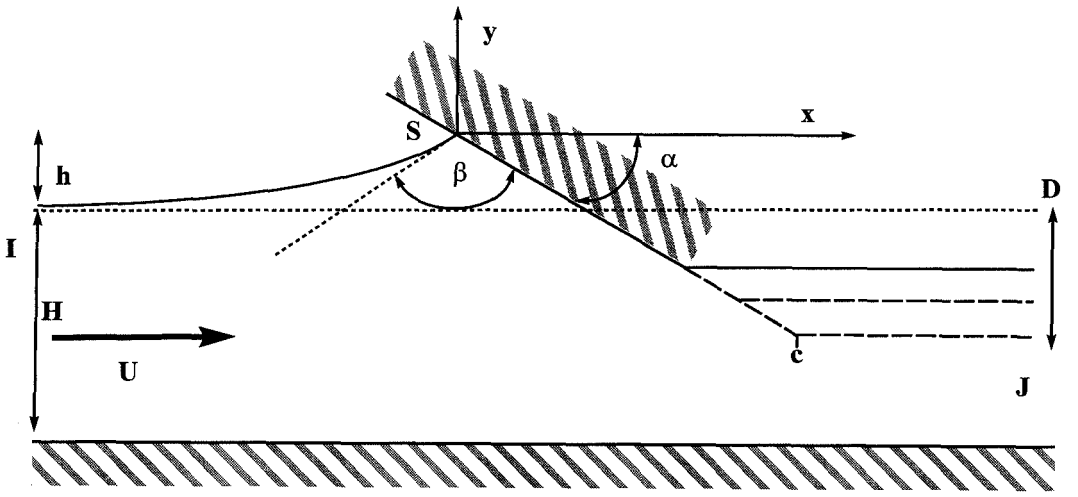

Figure 7.11: A sketch of the bow wave with variations in draft depth d .

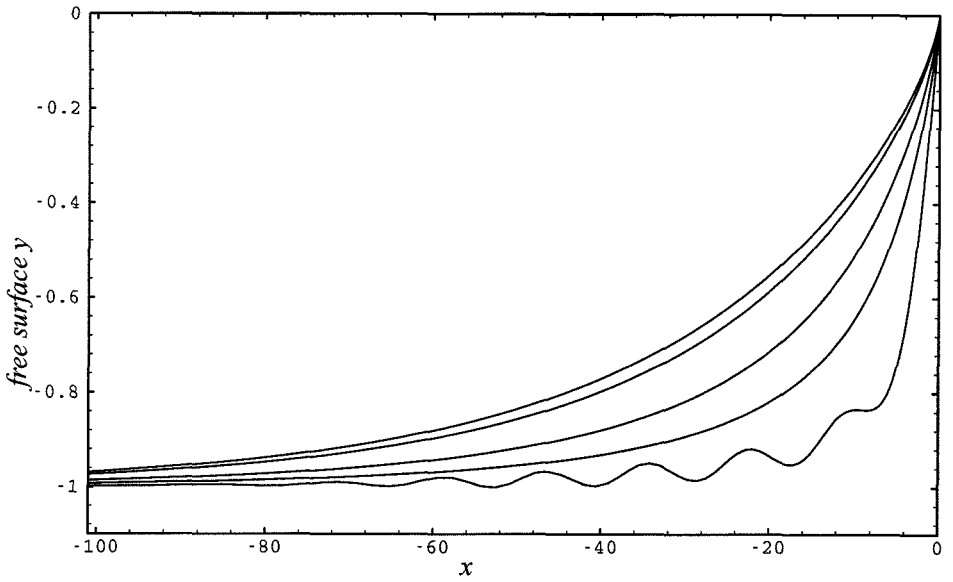

Figure 7.12: The effects due to variations in draft depth d on free surface shapes for $\alpha = 45°$, with $H = 100$, $d = 3$ (bottom), $9, 17, 40, 70$ (top) , employing 2+30 modes of a_{mn}'s .

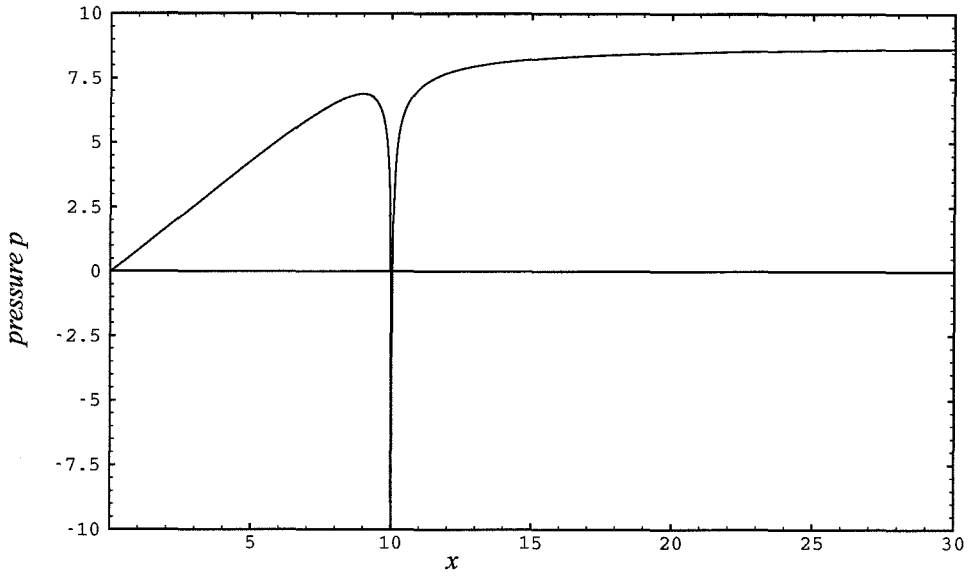

Figure 7.13: Pressure distribution over the bow plate and horizontal draft plate for $\alpha = 45°$, $H = 100$, $d = 9$, with 2+30 modes of a_{mn}'s , 341 grid points.

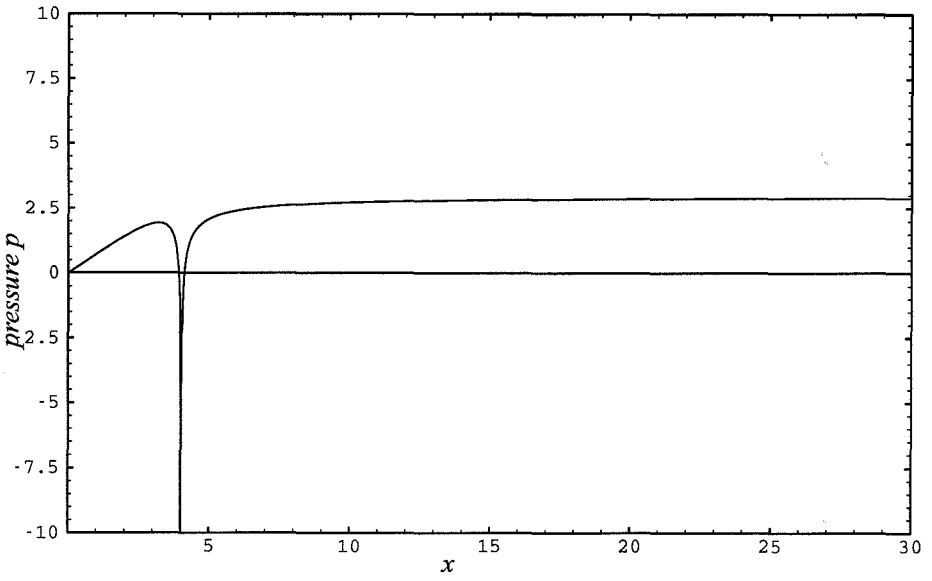

Figure 7.14: Pressure on the bow plate and horizontal draft plate for $\alpha = 45°$, $H = 100$, $d = 3$, with 2+30 modes of a_{mn}'s , 341 grid points.

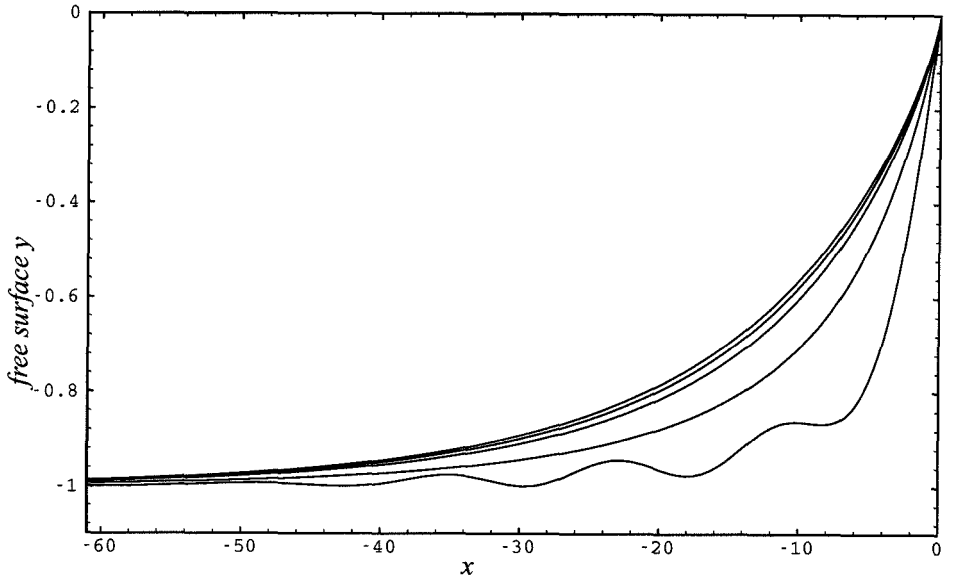

Figure 7.15: The effects due to variations in draft depth d on free surface shapes for $\alpha = 45°$, with $H = 50$, $d = 3$(bottom), $9, 17, 21, 25$ (top) , employing 2+30 modes of a_{mn}'s.

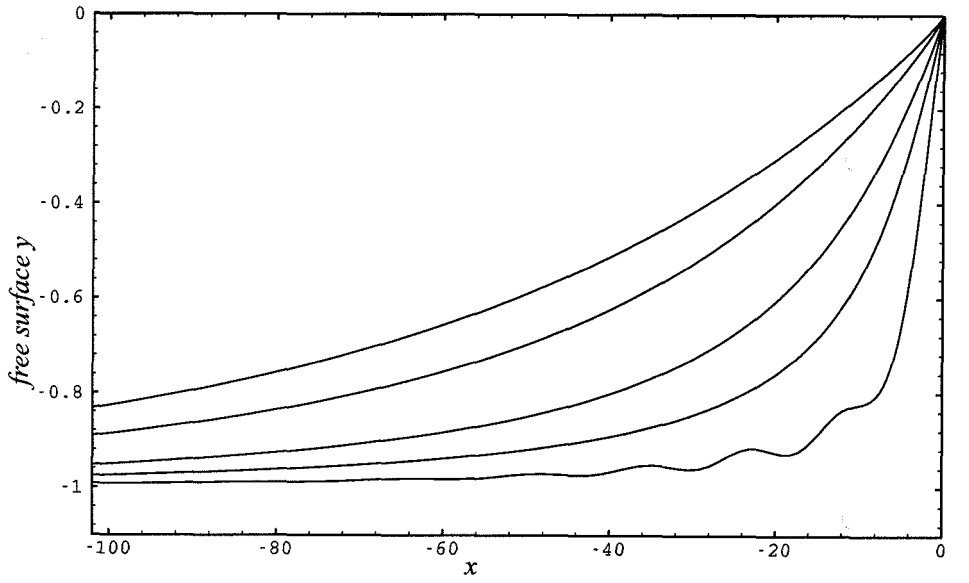

Figure 7.16: The effects due to variations in draft depth d on free surface shapes for $\alpha = 55°$, $H = 200$, $d = 3$ (bottom), $9, 17, 40, 70$(top) , employing 4+30 modes of a_{mn}'s.

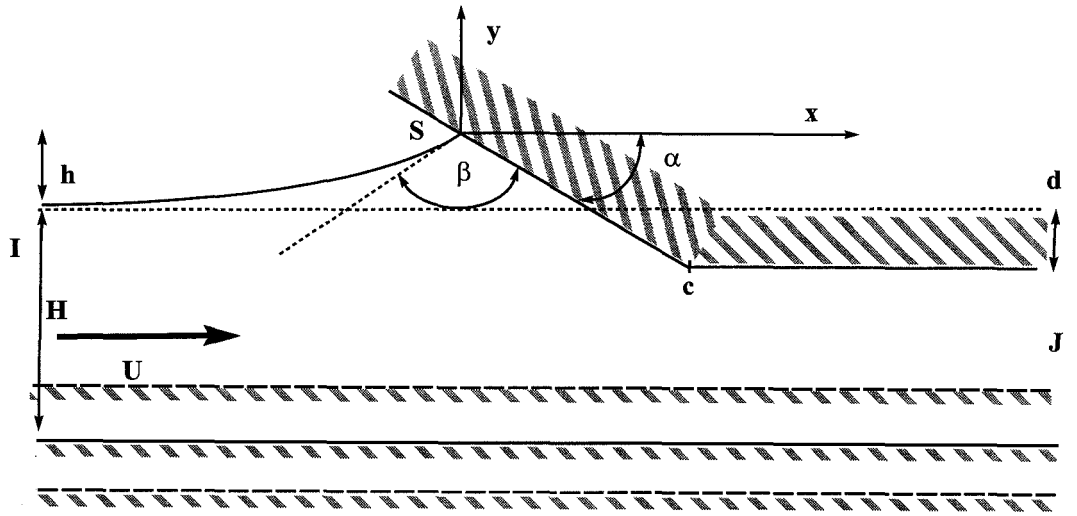

Figure 7.17: A sketch of the bow wave with variations in water depth H .

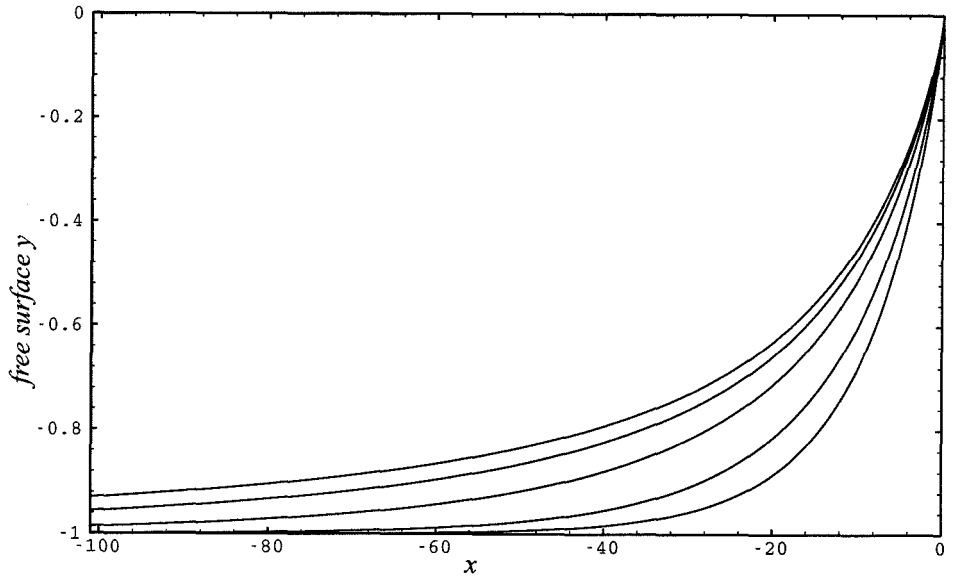

Figure 7.18: Variations of free-surface profile with varying water depth for $H =$ 35(bottom), 50, 100, 200, 400(top) , with $\alpha = 45°$, $d = 17$, using 2+30 modes of a_{mn}'s.

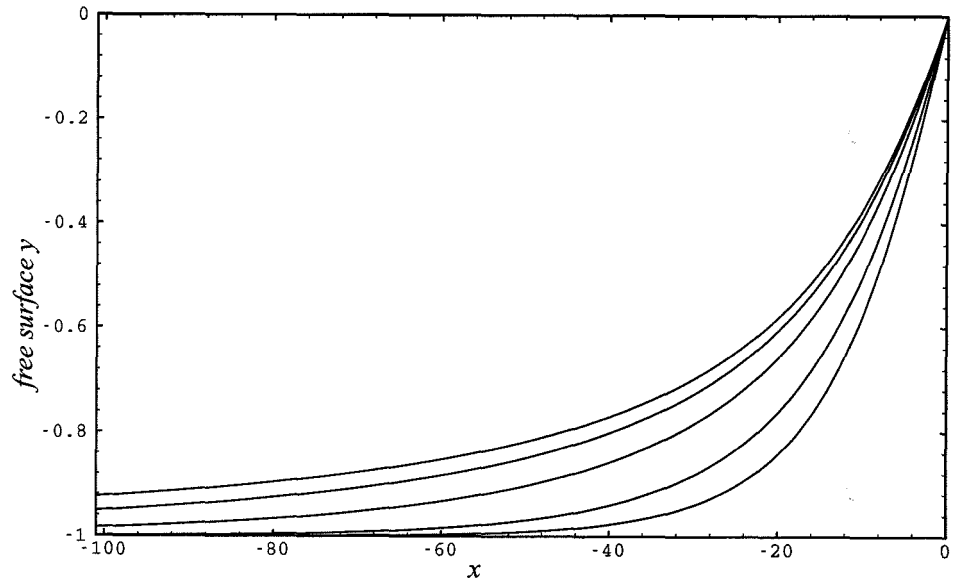

Figure 7.19: Variations of free-surface profile with varying water depth for $H =$ 35(bottom), 50, 100, 200, 400(top) , with $\alpha = 55°$, $d = 17$, using 4+30 modes of a_{mn}'s.

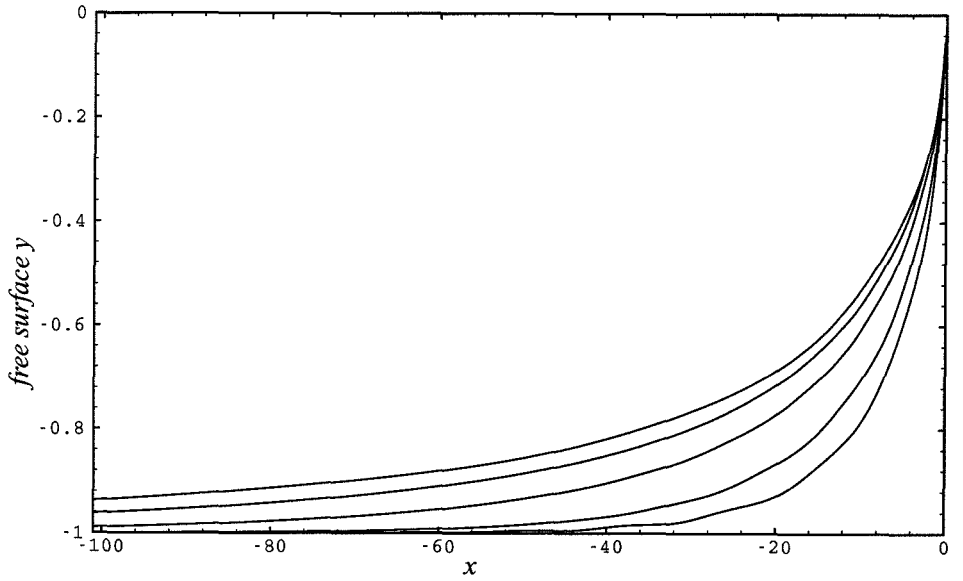

Figure 7.20: Variations of free-surface profile with varying water depth for $H =$ 35(bottom), 50, 100, 200, 400(top) , with $\alpha = 35°$, $d = 17$, using 2+30 modes of a_{mn}'s.

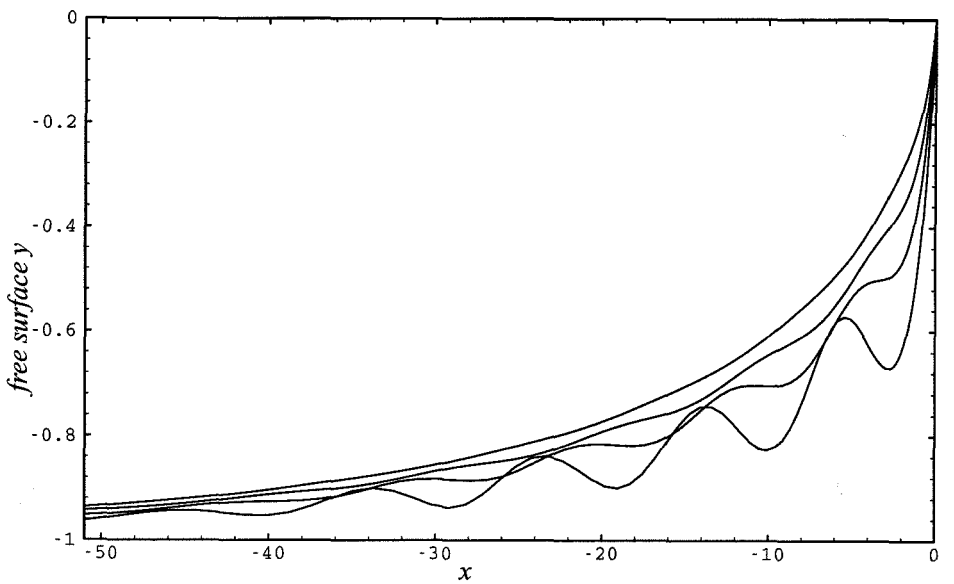

Figure 7.21: Variations of free-surface profile with varying the incidence angle for $\alpha = 22°$ (bottom), $27°, 31°, 35°$(top) , with $H = 100$, $d = 17$, using 2+30 modes of a_{mn}'s.

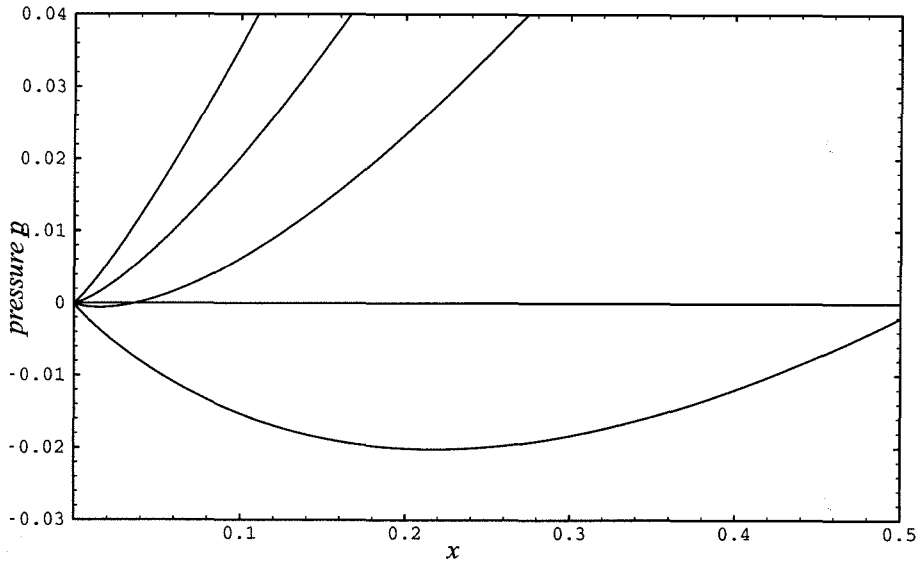

Figure 7.22: Variations of the pressure distributions in a neighborhood of the stagnation point with varying the incidence angle for $\alpha = 22°$ (bottom), $27°, 31°, 35°$(top) , with $H = 100$, $d = 17$, using 2+30 modes of a_{mn}'s.

	α	d	H	Fr_d	Fr_h	$Grid$	$M+N$	Dg_n	Dg_t
1	35	17	100	0.343	0.141	341	2+30	140.99827	141.01807
2	45	17	100	0.343	0.141	341	2+30	141.00881	141.01807
3	55	17	100	0.343	0.141	341	4+30	141.01358	141.01807
4	35	17	200	0.343	0.1	341	2+30	142.90836	142.92077
5	45	17	200	0.343	0.1	341	2+30	142.91461	142.92077
6	55	17	200	0.343	0.1	341	4+30	142.91762	142.92077
7	35	17	50	0.343	0.2	341	2+30	135.69028	135.74242
8	45	17	50	0.343	0.2	341	2+30	135.72198	135.74242
9	55	17	50	0.343	0.2	341	4+30	135.73353	135.74242

Table 7.1: Data for variations in the incidence angle α .

	α	d	H	Fr_d	Fr_h	$Grid$	$M+N$	Dg_n	Dg_t
1	45	3	100	0.816	0.141	341	2+30	4.40313	4.40722
2	45	9	100	0.471	0.141	341	2+30	39.60792	39.60989
3	45	17	100	0.343	0.141	341	2+30	141.00881	141.01807
4	45	40	100	0.224	0.141	341	2+30	773.19031	773.33333
5	45	70	100	0.169	0.141	341	2+30	2281.95097	2286.66667
6	45	3	50	0.816	0.2	341	2+30	4.30785	4.30851
7	45	9	50	0.471	0.2	341	2+30	38.52137	38.52439
8	45	17	50	0.343	0.2	341	2+30	135.72198	135.74242
9	45	21	50	0.309	0.2	341	2+30	205.24635	205.29310
10	45	25	50	0.283	0.2	341	2+30	287.39286	287.50000
11	55	3	200	0.816	0.1	341	4+30	4.45403	4.45431
12	55	9	200	0.471	0.1	341	4+30	40.07512	40.07592
13	55	17	200	0.343	0.1	341	4+30	142.91762	142.92077
14	55	40	200	0.224	0.1	341	4+30	789.97393	790.00000
15	55	70	200	0.169	0.1	341	4+30	2412.16485	2412.30769

Table 7.2: Data for variations in the draft depth d .

	α	d	H	Fr_d	Fr_h	$Grid$	$M+N$	Dg_n	Dg_t
1	45	17	35	0.343	0.239	341	2+30	128.39709	128.44444
2	45	17	50	0.343	0.2	341	2+30	135.72198	135.74242
3	45	17	100	0.343	0.141	341	2+30	141.00881	141.01807
4	45	17	200	0.343	0.1	341	2+30	142.91461	142.92077
5	45	17	400	0.343	0.071	341	2+30	143.74066	143.74543
6	55	17	35	0.343	0.239	341	4+30	128.42652	128.44444
7	55	17	50	0.343	0.2	341	4+30	135.73353	135.74242
8	55	17	100	0.343	0.141	341	4+30	141.01358	141.01807
9	55	17	200	0.343	0.1	341	4+30	142.91762	142.92077
10	55	17	400	0.343	0.071	341	4+30	143.74291	143.74543
11	35	17	35	0.343	0.239	341	2+30	128.29181	128.44444
12	35	17	50	0.343	0.2	341	2+30	135.69028	135.74242
13	35	17	100	0.343	0.141	341	2+30	140.99827	141.01807
14	35	17	200	0.343	0.1	341	2+30	142.90836	142.92077
15	35	17	400	0.343	0.071	341	2+30	143.73604	143.74543

Table 7.3: Data for variations in the water depth H .

	α	d	H	Fr_d	Fr_h	$Grid$	$M+N$	Dg_n	Dg_t
1	35	17	100	0.343	0.141	341	2+30	140.99827	141.01807
2	31	17	100	0.343	0.141	341	2+30	140.99057	141.01807
3	27	17	100	0.343	0.141	341	2+30	140.97856	141.01807
4	22	17	100	0.343	0.141	341	2+30	140.94953	141.01807

Table 7.4: Data for pressure variation near $\alpha = 30°$.

Chapter 8 Summary and Conclusion

In water of arbitrary finite depth, a fully nonlinear theoretical model of 2-D steady bow flow problem has been developed in this study for evaluating the incompressible irrotational flow satisfying the free-surface conditions and two constraint equations. The bow shape is assumed to consist of an inclined flat plate which has its lower edge connect to a horizontal draft plate, semi-infinite in length to downstream infinity. The bottom of the channel is assumed to be a horizontal plate. By applying the method of complex function, a complex velocity w is used to satisfy all the boundary conditions imposed on the flow. We apply a set of successive conformal transformation in the complex domain to map the flow domain into the interior of a unit semi-circle with its diameter corresponding to the solid boundaries and the semi-circle to the free surface. To choose the best form for the complex velocity w to incorporate into the full solutions, we analysis the local flows in a neighborhood of the stagnation point, the bow-draft corner and the upstream infinity, separately.

Our local flow analysis in the stagnation region shows that the wedge angle β between the free surface and the front bow plate must be equal to $120°$ for the incidence angle $0° < \alpha < 60°$. The pressure on the bow plate is positive for $30° < \alpha < 60°$, vanishes over the entire plate at $\alpha = 30°$ and becomes negative for $\alpha < 30°$. This implies that an appropriate suction on the bow plate is needed to prevent the negative pressure on the bow plate from happening. If no suction is provided on the bow plate, a local solution can only be existed for $30° < \alpha < 60°$;

otherwise, other types of flow might be possible. In addition, the higher order singularities of these local solutions in a neighborhood of the stagnation point and the upstream infinity are founded to have the branch-point singularities of irrational orders. We incorporate these singular structures into the full solution.

We represent the complex velocity w of the bow flow as a product of a known and an unknown velocities to satisfy the boundary conditions on the solid boundaries and on the free surface, respectively. The unknown velocity with its singular parts explicitly single out is represented by a series expansion. A set of non-linear equations in terms of the coefficients of the series is obtained by the method of minimization and solved by Newton's method.

By proceeding to compute the full solution of our model equations, we find that the incorporation of the singularities of irrational orders at the stagnation region and the upstream infinity into the full solution help greatly to improve the numerical convergence of the solution. Hence, only 30 coefficients of the series are needed for our calculation to reach an accuracy of 4 significant figures. In contrast, if the singularities of irrational orders are not included in our model, few hundreds or even thousands coefficients of the series are required for the convergence of our solution.

Comparing the two values of the drag obtained numerically and theoretically can check the accuracy of the solution. The values of the drags agree with each other to 4 significant figures.

Having established the fast-convergent and accurate numerical method, we proceed to investigate how the shape of free surface will vary with different values of the three parameters: the incidence angle α , the bow draft depth d and the

upstream water depth H .

First, we examine the effect due to variations in the incidence angle α while keeping the draft length d and water depth H fixed. The free surface profile falls off smoothly and monotonically to zero at the upstream infinity can be founded for $35° < \alpha < 60°$. On contrast, the free surface profile becomes wavy surface, a new type of solutions for $\alpha < 35°$. This bifurcation of solutions is due to the presence of a negative pressure in a neighborhood of the stagnation point on the bow plate around $\alpha = 30°$.

In addition, our results of monotonic and smooth solutions show that the free surface curve corresponding to the larger value of the angle of incidence α falls off to zero at a lower rate. This implies that the fluid at the stagnation region is pushed harder by the bow plate as α increases, but the flow must adjust itself for the drag D on the bow remaining unchanged.

Second, we examine the effect on the free surface profile due to variations in the draft depth d while keeping α and H fixed. If the solutions are monotonic and smooth for $Fr_d > 0.5$, the effects due to decreasing draft depth d are the following: the free surface falls off faster to zero, the magnitude of the drag on the bow becomes smaller, and the important of the negative pressure region at the bow-draft corner grows. The free surface profile becomes wavy surface for $Fr_d > 0.5$, which may be due to the effect of the negative pressure region at the bow-draft corner getting very close to the free surface.

Third, we study the effect on the free surface profile due to variations in the water depth H while keeping d and α fixed. We find that the monotonic and smooth free surface profile for $Fr_h < 0.4$. The effects due to the increasing

water depth are that the free surface falls off slower to zero, and the drag on the bow becomes larger. As the water depth H goes to infinity, we find no limiting free surface profile. This could be a primary reason for explaining the difficulties encountered in determining solution for the water of infinity depth.

Branch-point singularities of irrational orders exist in certain neighborhoods for other problems. For example, such singularities exist in the neighborhoods of the upstream and downstream infinities, given solitary water waves in water of arbitrary finite depth, including the highest solitary wave. In addition, such a branch-point singularity exists in a neighborhood of the stagnation point for the highest water waves, regardless of the water depth or the periodicity of the waves.

In our studies, we have found monotonic, smooth solutions for certain ranges of the parameters: α , H , and d . Further research outside these ranges is needed to find other forms of solutions, such as vortex flow, jet flow and unsteady flow. It has been reported other flow configurations may be feasible, such as a spray sheet forming at the bow plate and another kind with a forward recirculating vortex cell occurring at the free surface adjacent to the bow plate. The possibility of jet sheet formation is more likely at the high supercritical regime, a case which is not consider here. The recirculating vortex cell formation has been found to occur depending on the geometry configuration of the bow plate and its angle of inclination, as discussed by Dias & Vanden-Broeck (1993) and Miyata et al. (1984) . The result of our studies may be useful in bow shape design.

Bibliography

[1] Cole, S. L. & Strayer T. D. 1991 Free surface flow past a cylinder. In *Mathematical approaches in Hydrodynamics.* (ed. T. Miloh), pp. 193-206. SIAM

[2] Dagan, G. & Tulin, M. P. 1972 Two-dimensional free-surface gravity flow past blunt godies. *J. Fluid Mech.* **51**, 529-543.

[3] Dias, F. & Vanden-Broeck, J. M. 1993 Nonlinear bow flows with spray. *J. Fluid Mech.* **255**, 91-102.

[4] Farrow, D. E. & Tuck, E. O 1995 Further studies of stern wavemaking. *J. Austral. Math. Soc. Ser B* **36**, 424-437.

[5] Hocking, L. M. 1987 The damping of capillary-gravity waves at a rigid boundary. *J. Fluid Mech.* **179**, 253-266.

[6] Honji, H. 1976 Observation of a vortex in front of a half-submerged circular cylinder. *J. Phys. Soc. Japan.* , 1425-1478.

[7] Madurasinghe, M. A. & Tuck, E. O 1986 Ship bows with continuous and splashless flow attachment. *J. Austral. Math. Soc. Ser B* **27**, 442-452.

[8] Miyata, M. , Kajitani, H. , Matsukawa, C. , Suzuki, N. , Kanai, M. & Kuzumi, S. 1984 Numerical and Experimental Analysis of Nonlinear Bow and Stern Waves of A Two-dimensional Body. *J. of the Society of Naval Architects of Japan* **155**, 11-17.

[9] Olfe, D. B. & Rottman, J. W. 1980 Some new highest-wave solutions for deep-water waves of permanent form. *J. Fluid Mech.* **100**, 801-810.

[10] Teneda, S. 1974 Necklace Vortices. *J. Phys. Soc. Japan.* **36**(1), 298-303.

[11] Tuck, E. O & Vanden-Broeck, J.-M. 1985 Splashless bow flows in two dimensions?. In *Proc. 15nd Sym. Navl Hydrodynamics, Hamburg, 1984,* pp. 293-301. National Academy Press, Washington,DC.

[12] Vanden-Broeck, J.-M. 1986 Steep gravity waves: Havelock's method revisited. *Phys. Fluids.* **29**, 3084-3085.

[13] Vanden-Broeck, J.-M. 1989 Bow flows in water of finite depth. *Phys. Fluids.* A **1**, 1328-1330.

[14] Vanden-Broeck, J.-M. & Miloh, T. 1995 Computation of steep gravity waves by a refinement of Davis-Tulin's approximation. *SIMA J. Appl. Math.* **55**(4), 892-903.

[15] Vanden-Broeck, J.-M. , Schwartz, L. W. & Tuck, E. O. 1978 Divergent low-Froude-number series expansion in nonlinear free-surface flow problems. *Proc. R. Soc. Lond.* A **361**, 207-224.

[16] Vanden-Broeck, J.-M. & Tuck, E. O. 1977 Computation of near-bow or stern flows, using series expansion in the Froude number. In *Proc. 2nd Intl. Conf. Numerical Ships Hydrodynamics, Berkeley, CA,* pp. 371-381. University Extension Publications.

[17] Wagner, H. 1932 *ZAMM* vol. **12**, 193.

[18] Wu, D.-M. & Wu, T. Y. 1983 Three-dimensional nonlinear long waves due to moving surface pressure. *Proc. 14th Sym. Naval Hydrodynamics,* National Academic Press, Washington, D. C. , pp. 103-125.

[19] Wu, T. Y. T. 1967 Bow flows A singular perturbation theory for nonlinear free surface flow problems. *Intl. Shipbuild. Prog.* vol. **14**, 88-97.

[20] Yeung, R. W. 1991 Nonlinear bow waves-invicid and viscous solutions. In *Mathematical approaches in Hydrodynamics.* (ed. T. Miloh), pp. 349-369. SIAM